Isotopic evolution of the inner solar system revealed by size-dependent oxygen isotopic variations in chondrules

Yves Marrocchi, Alizé Longeau, Rosa Lozano Goupil, Valentin Dijon, Gabriel Pinto, Julia Neukampf, Johan Villeneuve, Emmanuel Jacquet

Isotopic evolution of the inner solar system revealed by size-dependent oxygen isotopic variations in chondrules

Yves Marrocchi[1,*], Alizé Longeau[1], Rosa Lozano Goupil[1], Valentin Dijon[1], Gabriel Pinto[1,2,3], Julia Neukampf[1], Johan Villeneuve[1] & Emmanuel Jacquet[2]

[1]Centre de Recherches Pétrographiques et Géochimiques (CRPG), CNRS, UMR 7358, Nancy, France
[2]Royal Belgian Institute of Natural Sciences, Geological Survey of Belgium, 1000, Brussels, Belgium
[3]Instituto de Ciencias de la Tierra, Universidad Austral de Chile, Valdivia, Chile.
[4]Institut de Minéralogie, de Physique des Matériaux et de Cosmochimie (IMPMC), Muséum national d'Histoire naturelle, Sorbonne Université, CNRS, CP52, 57 rue Cuvier, 75005 Paris, France.

*corresponding author: yvesm@crpg.cnrs-nancy.fr

Abstract

The systematic isotopic difference between refractory inclusions and chondrules, particularly for oxygen, has long indicated an isotopic evolution of the solar protoplanetary disk. However, it remains underconstrained whether such evolution continued during the chondrule formation epoch. Intrigued by past reports of the size-dependent oxygen isotopic compositions of chondrules in ordinary chondrites (OC), we analyzed type I olivine-rich chondrules of various sizes in two LL3 chondrites. Although most chondrules show positive $\Delta^{17}O$ values comparable to bulk ordinary chondrites, a population of smaller (less than about 0.1 mm² in cross-section), including many isolated olivine grains (*sensu lato*), are ^{16}O-enriched (with $\Delta^{17}O$ values down to −13.2 ‰). Literature data allow the same observation for R chondrites. All sub-TFL type I chondrules (i.e., $\Delta^{17}O < 0$) chondrules have Mg# > 97 mol% while the supra-TFL type I chondrule olivines extend to the formal boundary with type II chondrules (i.e., Mg# = 90 mol%). The sub-TFL chondrules are likely genetically related to isotopically similar aluminum-rich chondrules described in the literature. They therefore must have formed earlier than most OC and R chondrules when the inner disk was still sub-TFL. This interpretation is supported by the presence of similarly ^{16}O-rich relict grains in supra-

TFL OC and R chondrules that must be remains of this incompletely recycled precursor material. The non-carbonaceous reservoir was thus still evolving isotopically towards ^{16}O-poorer composition when chondrule formation began, whether by mixing with outer disk material, late accretion streamers and/or an increase in the solid/gas ratio due to magnetothermal disk winds.

Keywords: chondrules, oxygen isotopes, protoplanetary disk, dust dynamic, relict olivines

1- Introduction

The solar protoplanetary disk (PPD) surrounded the Sun for a few million years (e.g., Weiss et al. 2021) and was the site of an efficient production of submillimeter- to centimeter-scale solids that subsequently agglomerated into planetary bodies. The initial isotopic composition of the PPD was recorded by early refractory condensates in the form of calcium-aluminum-rich inclusions (CAIs) and ameboid olivine aggregates (AOAs). Their characterization has revealed that the disk was initially enriched in oxygen-16 ($\Delta^{17}O = \delta^{17}O - 0.52 \times \delta^{17}O < -20$ ‰; Krot, 2019; Marrocchi et al., 2019a) and neutron-rich *r*-process-derived nuclides (e.g., ^{48}Ca, ^{50}Ti, ^{54}Cr, and Mo and Ni isotopes; Trinquier et al., 2007, 2009; Burkhardt et al., 2021, Jansen et al., 2024, Torrano et al., 2024). Although CAIs and AOAs are generally considered to have condensed within 1 astronomical unit (AU, the semimajor axis of Earth's orbit, ~150×10^6 km; Jacquet, 2019; Bekaert et al. 2021), both are mostly observed in carbonaceous chondrites (CCs), whose parent bodies likely accreted in the outer solar system (Kruijer et al., 2017). This has been attributed to viscous expansion of the disk (e.g., Jacquet et al., 2011; Pignatale et al., 2019) or a dust trap outside a Jupiter-carved gap (Desch et al., 2018; Jongejan et al., 2023). Conversely, non-carbonaceous chondrites (NCs), thought to have accreted in the inner solar system, are notably depleted in refractory inclusions (Haugbølle et al., 2019; Dunham et al., 2023). Therefore, the isotopic compositions of CCs were more influenced by early-formed solids during disk evolution (Warren, 2011; Bryson and Brennecka, 2021; Marrocchi et al., 2023), yet also evidence a shift during PPD evolution.

Chondrules are submillimeter-scale igneous spheroids mostly composed of silicate minerals, glassy mesostases, Fe-Ni metal beads and sulfides. They represent the most

abundant high-temperature material in all types of chondrites, implying that both the inner and outer solar system were affected by their formation. Although the timing of the onset of chondrule formation remains debated (Bollard et al., 2017; Fukuda et al., 2022; Piralla et al., 2023), all chronometers indicate formation processes spanning several million years. Chondrules thus represent powerful proxies for quantifying the temporal isotopic evolution of the disk.

Recent characterizations of individual chondrules have revealed drastic differences between NC and CC chondrules: NC chondrules have homogeneous ε^{50}Ti and ε^{54}Cr values similar to those of their host chondrites (despite exceptions in EH3 chondrite Sahara 97096, Zhu et al., 2020), whereas CC chondrules have more variable values that sometimes greatly differ from those of their host chondrites while also being systematically lower than those of refractory inclusions (Gerber et al., 2017; Schneider et al., 2020). Furthermore, ^{16}O-rich relict olivine grains inherited from chondrule precursors are more abundant in CC chondrules (outside the CRHB clan; Marrocchi et al. 2022) than in their OC or R counterparts (Tenner et al., 2018; Marrocchi et al., 2018, 2019b; Regnault et al., 2022). This multi-isotope approach indicates that CC chondrules must have derived from the recycling of nebular condensates (Marrocchi et al., 2018, 2019b; Ebert et al., 2018, Williams et al., 2020), not from NC chondrule precursors as concluded from single-element isotopic data (Olsen et al., 2016; van Kooten et al., 2021). These results also imply that the isotopic composition of the disk changed rapidly after CAI and AOA condensation, settling towards values close to those sampled by NC chondrules (Brennecka et al., 2020). This could have occurred by intra-disk mixing (e.g., Jacquet et al., 2019) and/or the late infall of isotopically distinct material from the surrounding molecular cloud (Nanne et al., 2019; Burkhardt et al., 2019, 2021, Jansen et al., 2024). In the latter scenario, the varied isotopic compositions of CC chondrules would represent a mixture between (i) a CAI-AOA-like dust component recording the initial disk

131 composition and (ii) NC-like dust inherited from late infalling material from the molecular
132 cloud (Schneider et al., 2020).

133 Compared to CC chondrules, NC chondrules show a narrower range of
134 nucleosynthetic anomalies, suggesting they formed from different precursors and/or under
135 different conditions (Schneider et al., 2020). Although less abundant than in CC chondrules,
136 relict olivine grains with chemical signature similar to those in AOAs are observed in ordinary
137 chondrites (OCs, the most NCs; Kita et al., 2010; Piralla et al., 2021). This suggests that the
138 NC chondrules could have originated from AOA-like material that condensed after the
139 isotopic composition of the disk had shifted toward NC values (Brennecka et al., 2020; Piralla
140 et al., 2021). The preservation of early-formed refractory inclusions in the inner disk is not
141 trivial, however, as they would have either been lost to the Sun or rapidly accreted into
142 planetesimals (Spitzer et al., 2020). However, such early planetesimals would have melted
143 due to ^{26}Al decay, homogenizing their isotopic compositions and erasing any record of early
144 ^{16}O-rich material. The chondrule isotopic variability is not limited to rare relicts isotopically
145 similar to AOAs. Less ^{16}O-rich relict grains also occur and some OC chondrules are ^{16}O-
146 enriched relative to NC bulks (Kita et al., 2010; Piralla et al., 2021). In addition, separated
147 chondrules in unequilibrated OCs show systematically decreasing Δ^{17}O values with
148 decreasing chondrule size (Clayton et al., 1991). Therefore, the inner disk was certainly
149 populated by isotopically diverse dust populations that escaped sunward drift and melting in
150 planetesimals.

151 To better understand the nature of OC chondrule precursors, we selected variably sized
152 type I porphyritic olivine (PO) chondrules from the pristine OCs Piancaldoli (LL3.10;
153 Marrocchi et al., 2020) and NWA 5206 (LL3.05; Pape et al., 2019). We report a
154 comprehensive study of chondrule olivine grains combining petrological observations and
155 quantitative geochemical analyses. Based on our results, we discuss (i) the oxygen isotopic

156 variability of OC chondrule precursors, (ii) the conditions of OC chondrule formation, and
157 (iii) implications for dust dynamics and evolution in the inner solar system.
158
159 **2- Material & methods**
160
161 We surveyed all type I chondrules and isolated olivine grains (IOGs; Jacquet et al.,
162 2021) in two sections of the OC LL3.1 Piancaldoli: thin section USNM 5649 from the
163 National Museum of Natural History, Smithsonian Institution (Washington D.C., USA) and a
164 thick section prepared at the Centre de Recherches Pétrographiques et Géochimiques (CRPG-
165 CNRS, Nancy, France) from a parent sample provided by the Dipartimento scienze della Terra
166 e del Mare (Palermo, Italy). We also examined three thick sections of OC LL3.05 NWA 5206
167 that were prepared in-house. Chondrules were examined microscopically under transmitted
168 and reflected light. Among all porphyritic type I chondrules examined, we selected 47 olivine-
169 rich chondrules and IOGs with crystals large enough for major, minor, and trace element as
170 well as O isotopic analyses. The exposed surface areas of the chondrules were measured using
171 ImageJ (Schindelin et al., 2012, Pinto et al., 2021).
172 Scanning electron microscope observations were performed at CRPG-CNRS using a
173 JEOL JSM-6510 with 3 nA primary beam at 15 kV. We also performed multi-element EDX
174 mapping (Mg, Si, Fe, Ni, S, Na, Ca, and Al) of selected chondrules (Figs 1−3). Quantitative
175 point analyses were performed at the CRPG-CNRS using a JEOL JXA-8230 electron
176 microprobe analyzer (EPMA) equipped with five wavelength-dispersive spectrometers
177 (WDS) and one silicon drift detector energy dispersive spectrometer. Quantitative analyses of
178 Al, Ti, Ca, Cr, Mn, Ni, Mg, Fe, and Si in all olivine grains large enough to be isotopically
179 characterized by SIMS were performed with an accelerating voltage of 20 kV, a probe current
180 of 10 nA and beam diameter of 1 µm. We used different standards for tuning the EPMA:

Springwater olivine (Mg, Si), fayalite (Fe), wollastonite (Ca), albite (Na, Al), rutile (Ti), Ni metal (Ni), chromite (Cr) and rhodochrosite (Mn). The total peak + background counting time was 200 ms for Al, Ti, Ca, Mn and Cr, and 20 ms for Mg, Fe and Si. Detection limits were 0.025 wt% (Mg), 0.025 wt% (Fe), 0.05 wt% (Si), 0.005 wt% (Ca), 0.02 wt% (Al), 0.005 wt% (Ti), 0.015 wt% (Cr), and 0.008 wt% (Mn).

The oxygen isotopic compositions were measured by secondary ion mass spectrometry (SIMS) using a CAMECA IMS 1270 E7 at CRPG-CNRS (Bouden et al., 2021; Morin et al., 2022). $^{16}O^-$, $^{17}O^-$, and $^{18}O^-$ ions produced by a Cs^+ primary ion beam (~4 μm, 500 pA) were measured in multi-collection mode using two off-axis Faraday cups (FCs) for $^{16,18}O^-$ and the axial electron multiplier (EM) for $^{17}O^-$. To remove $^{16}OH^-$ interference on the $^{17}O^-$ peak and achieve maximum flatness atop the $^{16}O^-$ and $^{18}O^-$ peaks, the entrance and exit slits of the central EM were adjusted to achieve a mass resolving power (MRP = $M/\Delta M$) of ~6,000 for $^{17}O^-$. The OH contribution was negligible (< 0.1 %) and the ^{16}OH interference was well resolved. The multi-collection FCs were set on exit slit 1 (MRP = 2,500). The total measurement duration was 260 s, comprising 60 s of pre-sputtering and 200 s of measurement. Three terrestrial standard materials (San Carlos olivine, Ipanko spinel, and Rockport fayalite) were used to define the instrumental mass fractionation (IMF) line for the three oxygen isotopes and correct for IMF due to matrix effects in olivine. To monitor any instrumental drift and to achieve good precision, the San Carlos olivine was reanalyzed after every 10 sample analyses. Oxygen isotopic compositions are expressed in δ notation as $\delta^{17,18}O = ([^{17,18}O/^{16}O]_{sample}/[^{17,18}O/\ ^{16}O]_{V\text{-}SMOW} - 1) \times 1{,}000‰$, where V-SMOW refers to the Vienna Standard Mean Ocean Water. Samples related by mass-dependent fractionation to the V-SMOW composition plot along a line with a slope of 0.52, defining the terrestrial fractionation line (TFL), whereas mass-independent variations are described by $\Delta^{17}O = \delta^{17}O - 0.52 \times \delta^{18}O$, representing vertical deviations from the TFL in a triple oxygen isotope diagram.

Typical 2σ uncertainties, accounting for internal errors on each measurement and the external reproducibility of the standard, were estimated to be ~0.4‰ for $\delta^{18}O$, ~0.7‰ for $\delta^{17}O$, and ~0.8‰ for $\Delta^{17}O$. The error on $\Delta^{17}O$ was calculated by quadratically summing the errors on $\delta^{17}O$ and $\delta^{18}O$. All SIMS analytical spots were checked thoroughly by SEM, and any spots near fractures, in the mesostasis, or not completely within olivine grains were excluded from the data set (see Supplementary Materials).

3- Results

The 47 selected type I PO chondrules and IOGs have surface areas ranging from 0.005 to 0.87 mm^2. All contained euhedral to rounded olivine crystals with varying sizes in the range 15–75 µm (Figs. 1−3). Many of the smaller chondrules were IOGs in the broader sense of Jacquet et al. (2021), i.e., their olivines were dominated by a single crystal, even though they may also have contained other phases such as glassy mesostasis (Figs. 1−2). Larger *bona fide* chondrules (i.e., non-IOG) show palissadic textures (e.g., Libourel and Portail, 2018; Marrocchi et al., 2019b) with larger olivine grains occurring in the chondrule edges and smaller olivine crystals in chondrule interiors (Fig. 3). Punctual analyses in olivine show large variations in minor and trace elements, with Al_2O_3 ranging from 0.01 to 0.54 wt%, Cr_2O_3 from 0.03 to 1.01 wt%, MnO from 0.01 to 0.66 wt%, CaO from 0.03 to 0.81 wt% and TiO_2 from 0.01 to 0.16 wt% (Table S1). The Mg# (=Mg/(Mg + Fe) in mol%) of olivine grains range from 89.4 to 99.5 mol% (Table S1).

Olivine O-isotopic compositions vary widely, with $\delta^{18}O$ and $\delta^{17}O$ values ranging from −19 ‰ to 8.4 ‰ and from −23.4 ‰ to 6.1 ‰, respectively (Figs 4−5, S1−S41). Our set of data defines two isotopic populations that plot parallel to either the TFL (Fig. 5, average $\Delta^{17}O$ = 0.8 ± 0.6 ‰) or the Primary Chondrule Minerals line, (Fig.5; Ushikubo et al., 2012; $\Delta^{17}O$ =

231 −3.3 ± 2.8 ‰). Hereafter, we will refer to these populations as the *supra-TFL* and *sub-TFL*
232 populations, respectively. Individual chondrules generally showed uniform $\Delta^{17}O$, consistent
233 with the paucity of isotopically identifiable relicts reported by Piralla et al. (2021) in their
234 LL3 chondrites. The smallest supra-TFL chondrules (in 2D) show the isotopically lightest
235 mean compositions; possibly they were sectioned close to their surface as Piralla et al. (2021)
236 reported the isotopically heaviest spots to be concentrated in chondrule interiors. However,
237 half (6/12) of the sub-TFL chondrules show standard deviations (largely) beyond the
238 analytical precision (Fig. 6).

239 Our data define orthogonal relationships between $\Delta^{17}O$ and Mg# (Fig. 6A), as well as
240 minor and trace element concentrations (Figs. 6B−F). This trend is somewhat reminiscent of
241 the anticorrelation between $\Delta^{17}O$ and Mg# in CC chondrules (e.g., Chaumard et al., 2021,
242 Tenner et al., 2015, 2018 and references therein); here, however, the trend is not monotonic,
243 but rather the concatenation of two trends, one vertical and one horizontal, with no Mg# gap
244 (Fig. 6). All sub-TFL (i.e., $\Delta^{17}O < 0$) chondrules are restricted to Mg# > 97 mol% but span a
245 large range of $\Delta^{17}O$ values, whereas supra-TFL type I chondrule olivines span only a small
246 range of $\Delta^{17}O$ values but extend to the formal boundary with type II chondrules at Fo_{90} (i.e.,
247 Mg# = 90 mol%; Fig. 6A). This is in line with the relative Mn and Cr enrichment of supra-
248 TFL olivine, since these elements correlate positively with Fa content in chondrules in OCs
249 and elsewhere (e.g., Jacquet et al. 2015a). The highly magnesian compositions of the sub-TFL
250 chondrules are consistent with the observation of Pack et al. (2004) that 10 of 18 refractory
251 forsterites (cathodoluminescent, with Mg# > 98.3 mol%) in unequilibrated OCs (UOCs) were
252 sub-TFL.

253 Average $\Delta^{17}O$ values per chondrule also correlate with chondrule size; small
254 chondrules (especially below about 0.1 mm² in cross section) tend to be more enriched in ^{16}O
255 than larger chondrules (Fig. 7; Table S1). This is also true of literature data: we measured the

exposed areas of chondrules shown in published figures for both ordinary (Pack et al., 2004; Kita et al., 2010; Piralla et al., 2021; Ebert et al., 2022; Fig. 8) and Rumuruti chondrites (Pack et al., 2004; Regnault et al., 2022; Fig. 9), including Al-rich chondrules (Russell et al., 1996, 1998; Ebert et al., 2022). These results are consistent with the systematic decrease of $\Delta^{17}O$ values with decreasing chondrule size reported by Clayton et al. (1991) in H chondrites, although $\Delta^{17}O$ values remained positive for their finest size fractions (100-250 µm or 100-300 µm, about 0.01-0.1 mm²). Presumably, supra-TFL compositions remain dominant even for such size fractions (Fig. 7B).

Texturally, 4 out of our 12 sub-TFL chondrules are IOGs (Figs. 1,2); this is also true for 4 of the 14 (9 if considering only those with at least two analyses) sub-TFL chondrules of the extensive OC study of Baeza (2019). Earlier, Saxton et al. (1998) reported 5 sub-TFL compositions out of 7 coarse forsterites (IOG *sensu lato*) in the Julesburg L3.6 chondrite, consistent with the overrepresentation of IOGs among sub-TFL compositions.

4- Discussion

4.1 ^{16}O-rich OC chondrules: witnesses of a distinctive chondrule-forming reservoir

The most striking finding of our study is the correlation between chondrule size and oxygen isotopic composition (Figs 7–9). This leads us to consider two main types of chondrules: (i) sub-TFL chondrules (i.e., $\Delta^{17}O < 0$ ‰) and (ii) supra-TFL chondrules (i.e., $\Delta^{17}O \geq 0$ ‰). Straightforwardly, this correlation cannot be due to parent-body metamorphism because the smallest chondrules, which are more susceptible to re-equilibration, are isotopically furthest from the supra-TFL bulk OC chondrites/matrices (Clayton et al., 1991; Greenwood et al., 2020). It has been first suggested that all OC chondrules underwent

exchange with an ^{16}O-rich gas, and that the larger chondrules lagged nearer to their assumed (supra-TFL) starting isotopic composition due to their smaller surface/volume ratio (Clayton et al., 1986). However, these chondrules show little internal variation in the Δ^{17}O values of different phases (Kita et al., 2010), let alone olivine grains (with only 3 % of isotopically identifiable relicts; Piralla et al., 2021). Although sub-TFL aluminum-rich chondrules (ARCs) show isotopically distinctive mesostases, those mesostases are supra-TFL and were likely affected by incipient aqueous alteration, whereas other minerals mostly show indistinguishable Δ^{17}O values (Russell et al., 2000; Ebert et al., 2022). Therefore, there is no evidence for the mass-independent isotopic evolution of chondrule melts during the crystallization sequence of large supra-TFL chondrules. Conversely, the mass-dependent isotopic variations recorded by supra-TFL chondrules likely result from kinetic effects induced by evaporation/recondensation processes during the gas–melt interactions, possibly accumulated through successive recycling events (Piralla et al., 2021).

The fact remains that half of our sub-TFL olivine-rich type I chondrules show significant internal Δ^{17}O variations (Figs 4−8). The limited mass-dependent fractionation (with $\Delta^{18}O = \delta^{18}O - \delta^{17}O = 2.9 \pm 1.0$ ‰, Table S1) shown by sub-TFL chondrule suggests the heating timescale was much longer than the condensation timescale of oxygen, as maximum kinetic fractionation of order $[m(H_2{}^{17}O)/m(H_2{}^{16}O)]^{1/2} - 1 = 27$ ‰/amu could be produced (Cuzzi and Alexander, 2006). Consequently, the ambient gas should have significantly exchanged with sub-TFL chondrule melts before the onset of the crystallization of their host olivine grains.

The kinetics of oxygen isotopic exchange between CAI-like melts and O-bearing gas appear dominated by water vapor (Yamamoto et al., 2021, 2022). Using the 90 % exchange timescales reported for a 1 cm diameter molten CAI at 1540 °C (Yamamoto et al., 2021), we can correct for the size dependence for sub-mm molten chondrules (if we consider CAI melts

as suitable analogs of dry basaltic melts; Yamamoto et al. 2021). Beyond a critical water partial pressure (proportional to size) of ~0.1 Pa, the exchange timescale of a 0.5 mm diameter droplet (an upper bound for chondrules in this study) should be diffusion-limited at ~0.1 h (proportional to the square of the size). This is shorter than the day-scale cooling times estimated for type I chondrules (e.g., Jacquet et al. 2015a). Although the partial pressure of water in the OC chondrule-forming regions is not known, it appears that (i) the ratio to the total (H_2-dominated) pressure should be roughly enhanced by two orders of magnitude (e.g., Tenner et al. 2015) above the solar ratio (~10^{-3}; Yamamoto et al. 2021) and (ii) the total pressure would be ~1.4 Pa at 1 AU for a Minimum Mass Solar Nebula (Hayashi 1981). Thus, a value near the aforementioned critical value of ~0.1 Pa seems likely.

The host olivine crystals of sub-TFL chondrules thus record the average O-isotopic composition of their native reservoir, as do larger supra-TFL chondrules. This also implies that isotopically deviant grains in sub-TFL chondrules must be considered relicts from chondrule precursors, as are isotopically distinct grains in more classical NC and CC chondrules (e.g., Ruzicka et al., 2007; Ushikubo et al., 2012; Schrader et al., 2013; Tenner et al., 2013; Marrocchi et al., 2018, 2019b, 2022; Piralla et al., 2021; Schnuriger et al., 2022). However, the relict grains reported herein are not as ^{16}O-rich as AOAs (i.e., $\Delta^{17}O < -20‰$; Krot et al., 2004), instead forming a cluster of only relatively ^{16}O-rich compositions (Figs. 6–9). This indicates that the relicts in question must be relicts of pre-existing chondrules of the same general ^{16}O-rich reservoir (or, depending on how one delineates a reservoir, the set of ^{16}O-rich reservoirs sampled by sub-TFL chondrules). These ^{16}O-rich reservoir(s) must have spatially and/or temporally varied in composition for relicts to be isotopically manifest in recycled chondrules.

Therefore, we conclude that sub-TFL chondrules originated from a ^{16}O-rich reservoir, spatio-temporally distinct from that which formed most supra-TFL OC chondrules. We note

that the relicts found by (Piralla et al., 2021) in large supra-TFL chondrules span the same range of isotopic compositions and minor element abundances as the sub-TFL chondrules identified herein (with two isotopically AOA-like exceptions; Fig. 10). These relicts thus likely stem from preexisting sub-TFL chondrules. These must thus have been present in the OC-forming reservoir not only upon agglomeration, but also during the chondrule-melting events that produced larger supra-TFL chondrules. Because the reverse situation (*i.e.*, supra-TFL relicts within sub-TFL chondrules) is not observed, the sub-TFL chondrule-forming reservoir may have preceded the supra-TFL chondrule-forming (and accreting) one, consistent with the chronology suggested by Clayton et al., 1991. This is reminiscent of our results on CR chondrites supporting two generations of type I chondrules of distinct size distributions, further suggesting an evolution toward ^{16}O-poorer compositions (as exhibited by larger objects; Marrocchi et al., 2022). While Al-Mg dating on sub-TFL chondrules could test this inference, we found an initial $^{26}Al/^{27}Al$ estimate for only one such chondrule in the literature (c27 in NWA 8649; Siron et al. 2022), which, with $(7.52 \pm 0.88) \times 10^{-6}$, fits in the cluster of UOC chondrule ages, but its $\Delta^{17}O$ = -0.94 ‰ is only marginally in sub-TFL territory.

4.2 Significance of the small size of the *sub-TFL* chondrules

Because sub-TFL chondrules originate from a different reservoir than most OC chondrules, the difference in size compared to the latter may not be surprising as different chondrite groups show distinctive average sizes (e.g., Jones, 2012; Friedrich et al., 2015). However, it not obvious to what extent the observed size of these sub-TFL chondrules reflects that of their native population, because their sizes may have been biased by transport processes. Larger grains tend to drift faster than small grains (e.g., Jacquet et al., 2012); therefore the present-day sub-TFL chondrules may represent only the small end of a broader

size distribution, which could have diffused more efficiently across reservoirs (or have been depleted more slowly from a given evolving region of the disk).

As noted previously, we observed an overrepresentation of IOGs among the sub-TFL population (this study, Saxton et al., 1998; Pack et al., 2004). It was recently proposed that many IOGs showing evidence of interaction with a gas as single entities were expelled from colliding partially molten chondrules (Jacquet et al., 2021). A natural consequence of this process is to produce IOGs that are smaller than their parent chondrules (Jacquet et al., 2021). Such collisions could also occasionally expel olivine-free melt fragments that would solidify as spherical chondrules enriched in incompatible elements such as aluminum, calcium and sodium. Interestingly, most OC ARCs have sub-TFL compositions with similar size distributions and $\Delta^{17}O$ ranges as ferromagnesian sub-TFL chondrules (Fig. 8). Notably, Ebert and Bischoff (2016) mentioned splashing as a possible formation mechanism of ARCs. They nevertheless inferred that ARC had CAI-like precursors, drawing some analogy from their volatility-fractionated rare earth element patterns (Grossman et al., 1977, 1979). However, the REE patterns of ARCs are similar to those of enstatite chondrule mesostases, which were ascribed to igneous partitioning and are not diagnostic of CAIs (Jacquet et al., 2015b). In addition, OC CAIs have ^{50}Ti-rich compositions distinct from those of ARCs (Ebert et al., 2018). This lack of the hypothesized ARC CAI precursors is a serious issue given the nonnegligible abundance of ARCs. The latter may indeed be very roughly estimated from the (i) 30 ARCs in 15 OC sections studied by Ebert and Bischoff (2016) and (ii) an average apparent area of 0.14 mm² (Ebert et al., 2022). Assuming 1 cm^2 total area for each section (which will do for an order-of-magnitude estimate), this yields a modal abundance of 30 × 0.14 mm² / (15 × 1 cm²) = 0.3 %. Assuming 90 % recycling (i.e., an upper limit of the chondrule fraction in OCs) of these ARC-like CAIs exclusively in the form of ARCs, we would still expect ~0.03 % of isotopically ARC-like CAIs. This estimate is comparable to the

total abundance of CAIs reported in OCs (0.0088 %; Dunham et al., 2023), of which isotopically ARC-like ones must however be a very minor fraction, if at all extant.

Therefore, it is unlikely that CAI precursors can explain the composition of OC ARCs (unlike for CCs; Ebert et al., 2018), whereas their crystallization from residual melts enriched in incompatible elements is a much more generic process. We conversely hypothesize that most sub-TFL chondrules, whether ferromagnesian or aluminum-rich, represent melt splashes from partially molten droplets. Cold fragmentation is also conceivable because the correlation between size and isotopic compositions holds for fragments (Clayton et al., 1991). Sub-TFL chondrules may thus represent the smaller end of a broader size distribution of early-formed ^{16}O-rich chondrules, unless collisions from which they formed destroyed all larger droplets in their immediate region.

It is noteworthy that H chondrites have the smallest chondrules among UOCs, as well as the lowest bulk Δ^{17}O (0.69 ± 0.07 ‰ *vs.* 0.96 ± 0.11 ‰ in L chondrites and 1.08 ± 0.13 ‰ in LL chondrites; Clayton et al., 1991). As already suggested by Clayton et al. (1991), this may indicate a higher fraction (by a few percent) of small sub-TFL chondrules, resulting of differential size sorting in the OC-forming reservoir. Our observations are limited to LL chondrites, but we note that more abundant ARCs (mostly sub-TFL) were observed in H (22 in 8 thin sections) than in L and LL (8 in 7 thin sections) chondrites (Ebert and Bischoff, 2016), consistent with this expectation.

4.3 A carbonaceous chondrite provenance?

As chondrules in carbonaceous chondrites are generally ^{16}O-rich compared to their NC counterparts (e.g., Kita et al., 2010, Ushikubo et al. 2012; Tenner et al. 2015; Marrocchi et al. 2018, 2019, 2022, Piralla et al., 2021, Siron et al., 2022), this raises the question whether the

sub-TFL OC chondrules formed in the outer CC reservoir. There is some potential evidence for transport of NC chondrules to the C reservoir (e.g., Schrader et al. 2020; Williams et al. 2020), so migration in the other direction is conceivable. Al-Mg dating does not suggest CC chondrule formation to predate OC chondrule formation (e.g., Fukuda et al., 2022, Piralla et al. 2023), so there may be little prospect of significant drift of CC chondrules before the formation of the main population (supra-TFL) of OC chondrules. Yet Zhu et al. (2020) reported 2 chondrules with CC-like Cr isotopic composition out of 9 analyzed in EH3 chondrite Sahara 97096, although measurement of other isotopic systems would be desirable to exclude the possibility of a "lost component" in the inner disk (Burkhardt et al., 2021).

A first objection stems from the abundance of refractory inclusions in carbonaceous chondrites where a refractory inclusion/chondrule modal ratio ~0.1 is commonly reported (e.g., Jacquet et al. 2016; Ebel et al. 2016). Consequently, if some chondrules immigrated from the C reservoir, refractory inclusions must as well, especially since, being generally smaller than chondrules (May et al. 1999), they should not be preferentially filtered out by any size sorting, e.g. at a hypothetical pressure maximum (e.g., Haugbølle et al. 2019). However, the 0.001 vol% CAIs reported in subtype 3.00-3.2 UOCs (Dunham et al., 2023) provides an upper limit for the abundance of CAIs (+rare AOAs) coming from the C outer disk (and having escaped chondrule melting) there. Thus, using the refractory inclusion/chondrule ratio above, that of C-sourced chondrules cannot exceed ~0.01 vol%. The summed area of sub-TFL chondrules found in the 5 sections of this study is 1.4 mm^2 and the summed area of the said sections is 5.8 cm^2, thus representing an abundance of at least 0.2 vol% for our LL chondrites. This is a conservative lower bound, for our survey was not exhaustive (e.g., in being restricted to analyzable objects). Thus, sub-TFL chondrules appear too numerous to be cogenetic with any CC provenance subset of OC refractory inclusions.

Piralla et al. (2021) argued against a C provenance of sub-TFL relicts found in OC chondrules because their average $\Delta^{18}O$ was distinctly lower than CC host grains measured in the same laboratory (2.1 vs. 3.4 ‰). Our sub-TFL chondrules exhibit an average $\Delta^{18}O$ of 2.9 ‰, which, although consistent with the previous results, is no longer conclusive. Nevertheless, if we are right in associating sub-TFL ferromagnesian chondrules to sub-TFL ARC, the clearly NC isotopic composition of the latter (Ebert et al. 2018) also ties them to the NC superclan. We thus conclude that sub-TFL chondrules mostly formed in the NC reservoir, at an earlier time than most OC chondrules, although measurements of nucleosynthetic signatures in their ferromagnesian subset would be worthwhile.

4.4 Thermal, chemical and isotopic dynamics of the inner disk

The sub-TFL chondrules (including IOGs) studied herein commonly show diverse O isotopic compositions (Figs. 5–7). We propose that these chondrules correspond to the remains of a lost population of ^{16}O-rich large chondrules that initially populated the inner disk. Today, they are largely under-represented in OCs probably due to the sunward drift of most of their larger counterparts. Others were presumably recycled into supra-TFL chondrules, as attested by the sub-TFL nature of their relict olivine grains (Piralla et al., 2021; Fig. 10). This implies that recycling processes were highly efficient in the inner disk, as evidenced by the large modal abundance of supra-TFL chondrules in OCs. However, our study shows that some sub-TFL objects escaped remelting in supra-TFL environments, implying that both OC and R chondrites are composed of several genetically related chondrule populations formed at different times during the evolution of the inner disk. Furthermore, this attests of the nebular origin of OC and R chondrules because large planetary precursors (such as envisioned by Libourel and Krot 2007) would have been isotopically

455 homogenized by heat released from ^{26}Al-decay, which is inconsistent with the varied Δ^{17}O
456 values observed in sub-TFL chondrules and IOGs (Fig. 9). Interestingly, similar
457 interpretations were recently proposed in the CC reservoirs based on (i) the chemical
458 characteristics and oxygen isotopic compositions of relict olivine grains in type I CC
459 chondrules (Marrocchi et al., 2018, 2019b), (ii) the size-dependent oxygen isotope variations
460 observed in CR chondrules (Marrocchi et al., 2022), (iii) the presence of small ^{16}O-rich
461 chondrule-like objects in the Ryugu samples (Nakashima et al., 2023) and (iv) the similar
462 Δ^{17}O values observed between type I olivine phenocrysts and Mg-rich relict olivine grains in
463 type II chondrules (Pinto et al., 2024). Altogether, this evidence shows that the nebular dust
464 has been constantly reprocessed and recorded the evolving isotopic composition of the disk.
465 Combined with literature data, our results have profound implications on our
466 understanding of the evolution of the inner solar system. Assuming our "splash" hypothesis
467 for the formation of OC ARCs, the lost generation of inner disk chondrules were not
468 characterized by ^{50}Ti excesses. This supports models in which the initially *r*-process-rich
469 composition of the inner disk changed rapidly after being recorded by CAI condensation
470 (Nanne et al., 2019; Brennecka et al., 2020). Our data also show that sub-TFL chondrules and
471 IOGs have higher Mg# compared to supra-TFL chondrules (Figs 6−8). This highlights that
472 the isotopic composition and the redox state of the inner disk was still evolving from initially
473 ^{16}O-rich compositions and reduced conditions toward ^{16}O-poor, more oxidizing conditions
474 during chondrule formation. This interpretation is in line with the high modal abundance of
475 supra-TFL type II chondrules in ordinary chondrites (Tenner et al., 2018; Zanda et al. 2006).
476 In this regard, the presence of both reduced and oxidized supra-TFL chondrules within the
477 same OC does not imply their formation in two distinct spatial reservoirs.
478 The identification of the sub-TFL chondrule population attests to the isotopic
479 evolution of the inner disk. Because these objects recorded the isotopic compositions of their

480 formation reservoirs, the loss of some of them (e.g. the largest) by sunward drift should not
481 have generated any isotopic changes. This therefore suggests the addition of ^{16}O-poor material
482 after the condensation of ^{16}O-rich refractory inclusions. Such an addition might correspond to
483 ^{16}O-poor water ice resulting from CO self-shielding processes, either in the outer disk or in
484 the molecular cloud (e.g., Young et al. 2008). This water ice may have been enriched in
485 deuterium (Jacquet and Robert, 2013), which might account for the high D/H ratios of
486 minimally altered UOCs (Piani et al., 2021; Grant et al., 2023). Interestingly, the average ε^{50}Ti
487 of OC ARCs (i.e., −1.0 ± 0.1, Ebert et al., 2018), which are mostly sub-TFL, is slightly lower
488 than the bulk compositions of OCs (i.e., −0.66; Burkhardt et al., 2021). This may suggest a
489 late ^{50}Ti-rich admixture into the inner disk, which might correspond to CI-like dust. Indeed,
490 this scenario has recently been proposed to account for (i) bulk meteorite compositions
491 (Bryson & Brennecka, 2021, Yap and Tissot, 2023) and (ii) the evolution from type I-CO to
492 type I-CR chondrules in CR chondrites (Marrocchi et al., 2022).
493 Whatever the exact nature of the admixture, several astrophysical source can be
494 envisioned, such as (i) late accretion streamers onto the disk (e.g., Kuznetsova et al., 2022) or
495 (ii) material from the outer disk, whether drifting/diffusing freely or filtered by a gap carved
496 by Jupiter, with an outer pressure bump preventing the arrival of the coarsest solids (e.g.,
497 Haugbølle et al., 2019). Still, the mere change in composition of the solid assemblage cannot
498 intrinsically explain the trend toward more oxidized chondrule formation conditions, unless
499 invoking water-rich admixtures. This trend could be related to the solid/gas ratio (Tenner et
500 al., 2015; Marrocchi and Chaussidon, 2015), which might be increased by photoevaporation
501 of the gas-rich surface layers of the disk (e.g., Pascucci et al. 2022) or magnetized disk winds
502 (e.g., Borlina et al., 2021). Paleomagnetic records indicate the dissipation of the inner disk by
503 ~4 Ma after CAI formation (e.g., Borlina et al., 2021); associated effects on the solid/gas ratio

may thus have been appreciable by the time the later supra-TFL generation of NC chondrules formed.

5- Conclusions

We performed a petrographic, chemical and isotopic survey of type I porphyritic olivine-rich chondrules of various sizes in the unequilibrated ordinary chondrites Piancaldoli and NWA 5206. Our main results are:

1- Chondrules show large oxygen isotopic variations with $\delta^{18}O$ and $\delta^{17}O$ values ranging from −19 ‰ to 8.4 ‰ and from −23.4 ‰ to 6.1 ‰, respectively.

2- Among the studied chondrules, we observed two isotopic populations: small chondrules with heterogeneous mass-independent isotopic variations characterized by $\Delta^{17}O <$ 0‰ (n= 12) and their larger counterparts with homogeneous supra-TFL compositions (i.e., $\Delta^{17}O \geq 0$‰, n = 35).

3- Small chondrules have similar Mg# and minor element concentrations as relict olivine grains present within large supra-TFL chondrules.

From these observations, we propose the following interpretations:

1- Small sub-TFL chondrules (including aluminum-rich chondrules) originate from a ^{16}O-rich reservoir spatiotemporally distinct from that where supra-TFL OC chondrules formed. Sub-TFL chondrules thus represent a lost generation of chondrules that predates the formation of large supra-TFL chondrules.

2- Sub-TFL chondrules represent the small end of a broader size distribution of early-formed ^{16}O-rich chondrules. Their small size might result from their formation as fragments of collisions between partially molten ^{16}O-rich chondrules and/or differential loss by radial drift of their larger cogenetic counterparts.

3- Large supra-TFL chondrules formed through the recycling of this sub-TFL population in combination with gas-melt interactions.

4- The inner disk sampled by non-carbonaceous chondrites was still isotopically evolving toward ^{16}O-poorer composition at the onset of chondrule formation This could have resulted from the (i) injection of material from the molecular cloud or the outer disk or (ii) enhancement of the solid/gas ratio due to magnetothermal disk winds.

Acknowledgments

We thank Nordine Bouden for help during sample preparation and isotopic analyses. This work was funded by l'Agence Nationale de la Recherche through grant CASSYSS ANR-18-CE31-0010-01 (PI Johan Villeneuve). We thank the three anonymous reviewers for constructive comments and Associate Editor Frédéric Moynier for careful editing. This is CRPG contribution #2851.

Data Availability

Original data from this study are available on the Ordar database: https://doi.org/10.24396/ORDAR-123.

References

Baeza L (2019) Oxygen isotope systematics of ordinary chondrite chondrules: insights into the inner solar system planetary reservoir. Master of Philosophy of the Australian National University.

Bekaert D. V., Auro M., Shollenberger Q. R., Liu M.-C., Marschall H., Burton K. W., Jacobsen B., Brennecka G. A., McPherson G. J., von Mutius R., Sarafian A. and Nielsen S. G. (2021) Fossil records of early solar irradiation and cosmolocation of the CAI factory: A reappraisal. Sci. Adv. **7**, eabg8329.

Bollard J., Connelly J. N., Whitehouse M. J., Pringle E. A., Bonal L., Jørgensen J. K., Nordlund A, Moynier F. and Bizzarro M. (2017) Early formation of planetary building blocks inferred from Pb isotopic ages of chondrules. Science Advances 3, e1700407.

Borlina C. S., Weiss B. P., Bryson J. F. J., Bai X.-N., Lima E. A., Chatterjee N. and Mansbach E. N. (2021) Paleomagnetic evidence for a disk substructure in the early solar system. Science Advances 7, eabj6928.

Bouden N., Villeneuve J., Marrocchi Y., Deloule E., Füri E., Gurenko A., Piani L., Thomassot E., Peres P. and Fernandes F. (2021) Triple Oxygen Isotope Measurements by Multi-Collector Secondary Ion Mass Spectrometry. Frontiers in Earth Science 8, 9.

Brennecka G. A., Burkhardt C., Budde G., Kruijer T. S., Nimmo F. and Kleine T. (2020) Astronomical context of Solar System formation from molybdenum isotopes in meteorite inclusions. Science 370, 837–840.

Bryson J. F. J. and Brennecka G. A. (2021) Constraints on Chondrule Generation, Disk Dynamics, and Asteroid Accretion from the Compositions of Carbonaceous Meteorites. The Astrophysical Journal 912, 163.

Burkhardt C., Dauphas N., Hans U., Bourdon B. and Kleine T. (2019) Elemental and isotopic variability in solar system materials by mixing and processing of primordial disk reservoirs. Geochimica et Cosmochimica Acta 261, 145–170.

Burkhardt C., Spitzer F., Morbidelli A., Budde G., Render J. H., Kruijer T. S. and Kleine T. (2021) Terrestrial planet formation from lost inner solar system material. Science Advances 7, eabj7601.

Chaumard N., Defouilloy C., Hertwig A. T. and Kita N. T. (2021) Oxygen isotope systematics of chondrules in the Paris CM2 chondrite: indication for a single large formation region across snow line. Geochimica et Cosmochimica Acta 2021, 199-218.

Clayton R. N., Mayeda T. K. and Goswami J. N. (1986) Oxygen and Silicon Isotopic Variations in Chondrules. Meteoritics, 21, 346.

Clayton R. N., Mayeda T. K. and Goswami J. N. (1991) Oxygen isotope studies of ordinary chondrites. Geochimica et Cosmochimica Acta 55, 2317–2337.

Cuzzi J. N. and Alexander C. M. O. (2006) Chondrule formation in particle-rich nebular regions at least hundreds of kilometres across. Nature 441, 483–485.

Desch S. J., Kalyaan A. and Alexander C. M. O. (2018) The Effect of Jupiter's Formation on the Distribution of Refractory Elements and Inclusions in Meteorites. The Astrophysical Journal 238, 11.

Dunham E. T., Sheikh A., Opara D., Matsuda N., Liu M. - C. and McKeegan K. D. (2023) Calcium–aluminum- rich inclusions in non- carbonaceous chondrites: Abundances, sizes, and mineralogy. Meteoritics & Planetary Science 58, 643–671.

Ebert S. and Bischoff A. (2016) Genetic relationship between Na-rich chondrules and Ca,Al-rich inclusions? – Formation of Na-rich chondrules by melting of refractory and volatile precursors in the solar nebula. Geochimica et Cosmochimica Acta 177, 182–204.

Ebert S., Nagashima K., Bischoff A., Berndt J. and Krot A. N. (2022) Mineralogy, petrology, and oxygen isotopic compositions of aluminum-rich chondrules from unequilibrated

ordinary and the Dar al Gani 083 (CO3.1) chondrite. Geochimica et Cosmochimica Acta 336, 448–468.
Ebert S., Render J., Brennecka G. A., Burkhardt C., Bischoff A., Gerber S. and Kleine T. (2018) Ti isotopic evidence for a non-CAI refractory component in the inner Solar System. Earth and Planetary Science Letters 498, 257–265.
Friedrich J. M., Weisberg M. K., Ebel D. S., Biltz A. E., Corbett B. M., Iotzov I. V., Khan W. S. and Wolman M. D. (2015) Chondrule size and related physical properties: A compilation and evaluation of current data across all meteorite groups. Geochemistry 75, 419–443.
Fukuda K., Tenner T. J., Kimura M., Tomioka N., Siron G., Ushikubo T., Chaumard N., Hertwig A. T. and Kita N. T. (2022) A temporal shift of chondrule generation from the inner to outer Solar System inferred from oxygen isotopes and Al-Mg chronology of chondrules from primitive CM and CO chondrites. Geochimica et Cosmochimica Acta 322, 194–226.
Gerber S., Burkhardt C., Budde G., Metzler K. and Kleine T. (2017) Mixing and Transport of Dust in the Early Solar Nebula as Inferred from Titanium Isotope Variations among Chondrules. The Astrophysical Journal 841, L17.
Grant H., Tartèse R., Jones R., Piani L., Marrocchi Y., King A. and Rigaudier T. (2023) Bulk mineralogy, water abundance, and hydrogen isotope composition of unequilibrated ordinary chondrites. Meteoritics & Planetary Science 58, 1365–1381.
Greenwood R. C., Burbine T. H. and Franchi I. A. (2020) Linking asteroids and meteorites to the primordial planetesimal population. Geochimica et Cosmochimica Acta 277, 377–406.
Grossman L., Ganapathy R. and Davis A. M. (1977) Trace elements in the Allende meteorite—III. Coarse-grained inclusions revisited. Geochimica et Cosmochimica Acta 41, 1647–1664.
Grossman L., Ganapathy R., Methot R. L. and Davis A. M. (1979) Trace elements in the Allende meteorite—IV. Amoeboid olivine aggregates. Geochimica et Cosmochimica Acta 43, 817–829.
Haugbølle T., Weber P., Wielandt D. P., Benítez-Llambay P., Bizzarro M., Gressel O. and Pessah M. E. (2019) Probing the Protosolar Disk Using Dust Filtering at Gaps in the Early Solar System. The Astrophysical Journal 158, 55.
Jacquet E. (2019) Beryllium-10 production in gaseous protoplanetary disks and implications for the astrophysical setting of refractory inclusions. Astronomy and Astrophysics 624, A131-12.
Jacquet E., Alard O. and Gounelle M. (2015a) Trace element geochemistry of ordinary chondrite chondrules: The type I/type II chondrule dichotomy. Geochimica et Cosmochimica Acta 155, 47–67.
Jacquet E., Alard O. and Gounelle M. (2015b) The formation conditions of enstatite chondrites: Insights from trace element geochemistry of olivine-bearing chondrules in Sahara 97096 (EH3). Meteoritics & Planetary Science 50, 1624–1642.
Jacquet E., Fromang S. and Gounelle M. (2011) Radial transport of refractory inclusions and their preservation in the dead zone. Astronomy and Astrophysics 526, L8-4.
Jacquet E., Gounelle M. and Fromang S. (2012) On the aerodynamic redistribution of chondrite components in protoplanetary disks. Icarus 220, 162–173.
Jacquet E., Pignatale F. C., Chaussidon M. and Charnoz S. (2019) Fingerprints of the Protosolar Cloud Collapse in the Solar System. II. Nucleosynthetic Anomalies in Meteorites. The Astrophysical Journal 884, 32–11.
Jacquet E., Piralla M., Kersaho P. and Marrocchi Y. (2021) Origin of isolated olivine grains in carbonaceous chondrites. Meteoritics & Planetary Science 56, 13–33.
Jacquet E. and Robert F. (2013) Water transport in protoplanetary disks and the hydrogen isotopic composition of chondrites. Icarus 223, 722–732.

Jansen C. A., Burkhardt C., Marrocchi Y., Schneider J. M., Wölfer E. and Kleine T. (2024) Condensate evolution in the solar nebula inferred from combined Cr, Ti, and O isotope analyses of amoeboid olivine aggregates. Earth and Planetary Science Letters **627**, 118567.
Jones R. H. (2012) Petrographic constraints on the diversity of chondrule reservoirs in the protoplanetary disk. Meteoritics & Planetary Science 47, 1176–1190.
Jongejan S., Dominik C. and Dullemond C. P. (2023) The effect of Jupiter on the CAI storage problem. Astronomy and Astrophysics 679, A45.
Kita N. T., Nagahara H., Tachibana S., Tomomura S., Spicuzza M. J., Fournelle J. H. and Valley J. W. (2010) High precision SIMS oxygen three isotope study of chondrules in LL3 chondrites: Role of ambient gas during chondrule formation. Geochimica et Cosmochimica Acta 74, 6610–6635.
van Kooten E., Schiller M., Moynier F., Johansen A., Haugbølle T. and Bizzarro M. (2021) Hybrid Accretion of Carbonaceous Chondrites by Radial Transport across the Jupiter Barrier. The Astrophysical Journal 910, 70.
Krot A. N. (2019) Refractory inclusions in carbonaceous chondrites: Records of early solar system processes. Meteoritics & Planetary Science 54, 1647–1691.
Krot A. N., Petaev M. I., Russell S. S., Itoh S., Fagan T. J., Yurimoto H., Chizmadia L., Weisberg M. K., Komatsu M., Ulyanov A. A. and Keil K. (2004) Amoeboid olivine aggregates and related objects in carbonaceous chondrites: records of nebular and asteroid processes. Chemie der Erde - Geochemistry 64, 185–239.
Kruijer T. S., Burkhardt C., Budde G. and Kleine T. (2017) Age of Jupiter inferred from the distinct genetics and formation times of meteorites. Proc Natl Acad Sci USA, 201704461.
Kuznetsova A., Bae J., Hartmann L. and Low M.-M. M. (2022) Anisotropic Infall and Substructure Formation in Embedded Disks. The Astrophysical Journal 928, 92.
Libourel G. and Krot A. N. (2007) Evidence for the presence of planetesimal material among the precursors of magnesian chondrules of nebular origin. Earth and Planetary Science Letters 254, 1–8.
Libourel G., Nagashima K., Portail M. and Krot A. N. (2023) On the significance of oxygen-isotope variations in chondrules from carbonaceous chondrites. Geochimica et Cosmochimica Acta 346, 102–120.
Libourel G. and Portail M. (2018) Chondrules as direct thermochemical sensors of solar protoplanetary disk gas. Science Advances 4, eaar3321-32.
Marrocchi Y., Bonal L., Gattacceca J., Piani L., Beck P., Greenwood R., Eschrig J., Basque A., Nuccio P. M. and Martin F. F. (2020) The Piancaldoli meteorite: A forgotten primitive LL3.10 ordinary chondrite. Meteoritics & Planetary Science 55, 1924-1935.
Marrocchi Y. and Chaussidon M. (2015) A systematic for oxygen isotopic variation in meteoritic chondrules. Earth and Planetary Science Letters 430, 308–315.
Marrocchi Y., Euverte R., Villeneuve J., Batanova V., Welsch B., Ferrière L. and Jacquet E. (2019b) Formation of CV chondrules by recycling of amoeboid olivine aggregate-like precursors. Geochimica et Cosmochimica Acta 247, 121–141.
Marrocchi Y., Piralla M., Regnault M., Batanova V., Villeneuve J. and Jacquet E. (2022) Isotopic evidence for two chondrule generations in CR chondrites and their relationships to other carbonaceous chondrites. Earth and Planetary Science Letters 593, 117683.
Marrocchi Y., Piralla M. and Tissot F. L. H. (2023) Iron Isotope Constraints on the Structure of the Early Solar System. The Astrophysical Journal 954, L27.
Marrocchi Y., Villeneuve J., Batanova V., Piani L. and Jacquet E. (2018) Oxygen isotopic diversity of chondrule precursors and the nebular origin of chondrules. Earth and Planetary Science Letters 496, 132–141.

Marrocchi Y., Villeneuve J., Jacquet E., Piralla M. and Chaussidon M. (2019a) Rapid condensation of the first Solar System solids. Proceedings of the National Academy of Sciences of the United States of America 116, 23461–23466.

Morin G. L. F., Marrocchi Y., Villeneuve J. and Jacquet E. (2022) ^{16}O-rich anhydrous silicates in CI chondrites: Implications for the nature and dynamics of dust in the solar accretion disk. Geochimica et Cosmochimica Acta 332, 203–219.

Nakashima D., Nakamura T., Zhang M., Kita N. T., Mikouchi T., Yoshida H., Enokido Y., Morita T., Kikuiri M., Amano K., Kagawa E., Yada T., Nishimura M., Nakato A., Miyazaki A., Yogata K., Abe M., Okada T., Usui T., Yoshikawa M., Saiki T., Tanaka S., Nakazawa S., Terui F., Yurimoto H., Noguchi T., Yabuta H., Naraoka H., Okazaki R., Sakamoto K., Watanabe S., Tachibana S. and Tsuda Y. (2023) Chondrule-like objects and Ca-Al-rich inclusions in Ryugu may potentially be the oldest Solar System materials. Nature Communications 14, 532.

Nanne J. A. M., Nimmo F., Cuzzi J. N. and Kleine T. (2019) Origin of the non-carbonaceous–carbonaceous meteorite dichotomy. Earth and Planetary Science Letters 511, 44–54.

Olsen M. B., Wielandt D., Schiller M., Van Kooten E. M. M. E. and Bizzarro M. (2016) Magnesium and 54Cr isotope compositions of carbonaceous chondrite chondrules – Insights into early disk processes. Geochimica et Cosmochimica Acta 191, 118–138.

Pack A., Yurimoto H. and Palme H. (2004) Petrographic and oxygen-isotopic study of refractory forsterites from R-chondrite Dar al Gani 013 (R3.5–6), unequilibrated ordinary and carbonaceous chondrites. Geochimica et Cosmochimica Acta 68, 1135–1157.

Pape J., Mezger K., Bouvier A.-S. and Baumgartner L. P. (2019) Time and duration of chondrule formation: Constraints from ^{26}Al-^{26}Mg ages of individual chondrules. Geochimica et Cosmochimica Acta 244, 416–436.

Pascucci I., Cabrit S., Edwards S., Gorti U., Gressel O. and Suzuki T. (2022) The Role of Disk Winds in the Evolution and Dispersal of Protoplanetary Disks. Protostars and Planets VII, ASP Conference Series, Vol. 534, Proceedings of a conference held 10-15 April 2023 at Kyoto, Japan. Edited by Shu-ichiro Inutsuka, Yuri Aikawa, Takayuki Muto, Kengo Tomida, and Motohide Tamura. San Francisco: Astronomical Society of the Pacific, 2023, p.567

Piani L., Marrocchi Y., Vacher L. G., Yurimoto H. and Bizzarro M. (2021) Origin of hydrogen isotopic variations in chondritic water and organics. Earth and Planetary Science Letters 567, 117008.

Pignatale F. C., Jacquet E., Chaussidon M. and Charnoz S. (2019) Fingerprints of the Protosolar Cloud Collapse in the Solar System. I. Distribution of Presolar Short-lived ^{26}Al. The Astrophysical Journal 884, 31–8.

Pinto G. A., Marrocchi Y., Morbidelli A., Charnoz S., Varela M. E., Soto K., Martínez R., and Olivares F. (2021). Constraints on Planetesimal Accretion Inferred from Particle-size Distribution in CO Chondrites. *The Astrophysical Journal Letters* 917:L25.

Pinto G. A., Jacquet E., Corgne A., Olivares F., Villeneuve J. and Marrocchi Y. (2024) Deciphering recycling processes during solar system evolution from magnesium-rich relict olivine grains in type II chondrules. Geochimica et Cosmochimica *Acta* 364, 65–78.

Piralla M., Villeneuve J., Batanova V., Jacquet E. and Marrocchi Y. (2021) Conditions of chondrule formation in ordinary chondrites. Geochimica et Cosmochimica Acta 313, 295–312.

Piralla M., Villeneuve J., Schnuriger N., Bekaert D. V. and Marrocchi Y. (2023) A unified chronology of dust formation in the early solar system. Icarus 394, 115427.

Regnault M., Marrocchi Y., Piralla M., Villeneuve J., Batanova V., Schnuriger N. and Jacquet E. (2022) Oxygen isotope systematics of chondrules in Rumuruti chondrites: Formation

conditions and genetic link with ordinary chondrites. Meteoritics & Planetary Science 57, 122–135.
Russell S. S., MacPherson G. J., Leshin L. A. and McKeegan K. D. (2000) ^{16}O enrichments in aluminum-rich chondrules from ordinary chondrites. Earth and Planetary Science Letters 184, 57–74.
Russell S. S., Srinivasan G., Huss G. R., Wasserburg G. J. and MacPherson G. J. (1996) Evidence for Widespread ^{26}Al in the Solar Nebula and Constraints for Nebula Time Scales. Science 273, 757–762.
Ruzicka A., Hiyagon H., Hutson M. and Floss C. (2007) Relict olivine, chondrule recycling, and the evolution of nebular oxygen reservoirs. Earth and Planetary Science Letters 257, 274–289.
Saxton J. M., Lyon I. C. and Turner G. (1998) Oxygen isotopes in forsterite grains from Julesburg and Allende: Oxygen-16-rich material in an ordinary chondrite. Meteoritics & Planetary Science 33, 1017–1027.
Schindelin J., Arganda-Carreras I., Frise E., Kaynig V., Longair M., Pietzsch T., Preibisch S., Rueden C., Saalfeld S., Schmid B., Tinevez J.-Y., White D. J., Hartenstein V., Eliceiri K., Tomancak P. and Cardona A. (2012) Fiji: an open-source platform for biological-image analysis. Nat Methods 9, 676–682.
Schneider J. M., Burkhardt C., Marrocchi Y., Brennecka G. A. and Kleine T. (2020) Early evolution of the solar accretion disk inferred from Cr-Ti-O isotopes in individual chondrules. Earth and Planetary Science Letters 551, 116585.
Schnuriger N., Cartier C., Villeneuve J., Batanova V., Regnault M. and Marrocchi Y. (2022) Spinel in CV chondrules: Investigating precursor legacy and chondrule thermal histories. Meteoritics & Planetary Science 57, 1018–1037.
Schrader D. L., Connolly Jr H. C., Lauretta D. S., Nagashima K., Huss G. R., Davidson J. and Domanik K. J. (2013) The formation and alteration of the Renazzo-like carbonaceous chondrites II: Linking O-isotope composition and oxidation state of chondrule olivine. Geochimica et Cosmochimica Acta 101, 302–327.
Schrader D. L., Nagashima K., Davidson J., McCoy T. J., Ogliore R. C. and Fu R. R. (2020) Outward migration of chondrule fragments in the early Solar System: O-isotopic evidence for rocky material crossing the Jupiter Gap? Geochimica et Cosmochimica Acta **282**, 133–155.
Spitzer F., Burkhardt C., Budde G., Kruijer T. S., Morbidelli A. and Kleine T. (2020) Isotopic Evolution of the Inner Solar System Inferred from Molybdenum Isotopes in Meteorites. The Astrophysical Journal 898, L2.
Tenner T. J., Nakashima D., Ushikubo T., Kita N. T. and Weisberg M. K. (2015) Oxygen isotope ratios of FeO-poor chondrules in CR3 chondrites: Influence of dust enrichment and H_2O during chondrule formation. Geochimica et Cosmochimica Acta 148, 228–250.
Tenner T. J., Ushikubo T., Kurahashi E., Kita N. T. and Nagahara H. (2013) Oxygen isotope systematics of chondrule phenocrysts from the CO3.0 chondrite Yamato 81020: Evidence for two distinct oxygen isotope reservoirs. Geochimica et Cosmochimica Acta 102, 226–245.
Tenner, T. J., Ushikubo, T., Nakashima, D., Schrader, D. L., Weisberg, M. K., Kimura, M., & Kita, N. T. (2018). Oxygen Isotope Characteristics of Chondrules from Recent Studies by Secondary Ion Mass Spectrometry. In *Chondrules: Records of Protoplanetary Disk Processes*. Cambridge University Press, pp. 196–246.
Torrano Z. A., Alexander C. M. O., Carlson R. W., Render J., Brennecka G. A. and Bullock E. S. (2024) A common isotopic reservoir for amoeboid olivine aggregates (AOAs) and calcium-aluminum-rich inclusions (CAIs) revealed by Ti and Cr isotopic compositions. Earth and Planetary Science Letters **627**, 118551.

Trinquier A., Birck J. and Allegre C. J. (2007) Widespread ^{54}Cr Heterogeneity in the Inner Solar System. The Astrophysical Journal 655, 1179–1185.
Trinquier A., Elliott T., Ulfbeck D., Coath C., Krot A. N. and Bizzarro M. (2009) Origin of Nucleosynthetic Isotope Heterogeneity in the Solar Protoplanetary Disk. Science 324, 374–376.
Ushikubo T., Kimura M., Kita N. T. and Valley J. W. (2012) Primordial oxygen isotope reservoirs of the solar nebula recorded in chondrules in Acfer 094 carbonaceous chondrite. Geochimica et Cosmochimica Acta 90, 242–264.
Warren P. H. (2011) Stable-isotopic anomalies and the accretionary assemblage of the Earth and Mars: A subordinate role for carbonaceous chondrites. Earth and Planetary Science Letters 311, 93–100.
Weiss B. P., Bai X.-N. and Fu R. R. (2021) History of the solar nebula from meteorite paleomagnetism. *Sci. Adv.* **7**, eaba5967.
Williams C. D., Sanborn M. E., Defouilloy C., Yin Q.-Z., Kita N. T., Ebel D. S., Yamakawa A. and Yamashita K. (2020) Chondrules reveal large-scale outward transport of inner Solar System materials in the protoplanetary disk. Proc Natl Acad Sci USA **117**, 23426–23435.
Yamamoto D., Kawasaki N., Tachibana S., Kamibayashi M. and Yurimoto H. (2021) An experimental study on oxygen isotope exchange reaction between CAI melt and low-pressure water vapor under simulated Solar nebular conditions. Geochimica et Cosmochimica Acta **314**, 108–120.
Yamamoto D., Kawasaki N., Tachibana S., Kamibayashi M. and Yurimoto H. (2022) Oxygen isotope exchange kinetics between CAI melt and carbon monoxide gas: Implication for CAI formation in the earliest Solar System. Geochimica et Cosmochimica Acta **336**, 104–112.
Yap T. E. and Tissot F. L. H. (2023) The NC-CC dichotomy explained by significant addition of CAI-like dust to the Bulk Molecular Cloud (BMC) composition. Icarus 405, 115680.
Young E. D., Kuramoto K., Marcus R. A., Yurimoto H. and Jacobsen S. B. (2008) Mass-independent Oxygen Isotope Variation in the Solar Nebula. Reviews in Mineralogy and Geochemistry **68**, 187–218.
Zanda B., Hewins R., Bourot-Denise M., Bland P. and Alabarède F. (2006) Formation of solar nebula reservoirs by mixing chondritic components. Earth and Planetary Science Letters **248**, 650–660.
Zhu K., Moynier F., Schiller M. and Bizzarro M. (2020) Dating and Tracing the Origin of Enstatite Chondrite Chondrules with Cr Isotopes. The Astrophysical Journal 894, L26.

Figure caption

Fig 1: (A, C, E) Backscattered electron images of small olivine-rich porphyritic chondrules in chondrite NWA 5206. The average $\Delta^{17}O$ values of each chondrule are reported. (B, D, F) Compiled EDX maps of Si and Mg in the same three PO chondrules, revealing the mineralogy of the different chondrule silicate phases: olivines (orange), low-Ca pyroxenes (pale green), and mesostasis (dark green).

Fig 2: (A, C, E) Backscattered electron images of isolated olivine grains (IOGs) and small olivine-rich porphyritic chondrules in chondrites NWA 5206 and Piancaldoli. The average $\Delta^{17}O$ values of each chondrule are reported. (B, D, F) Compiled EDX maps of Si and Mg in the the IOG and two PO chondrules, revealing the mineralogy of the different chondrule silicate phases: olivines (orange), low-Ca pyroxenes (pale green), and mesostasis (dark green).

Fig 3: (A, C, E) Backscattered electron images of large olivine-rich porphyritic chondrules in chondrite NWA 5206. The average $\Delta^{17}O$ values of each chondrule are reported. (B, D, F) Compiled EDX maps of Si and Mg of PO chondrules, revealing the mineralogy of the different chondrule silicate phases: olivines (orange), low-Ca pyroxenes (pale green), and mesostasis (dark green).

Fig 4: Oxygen three-isotope diagrams for different type I chondrules of varying sizes in the OC chondrites Piancaldoli and NWA 5206. Chondrules show (i) homogenous supra-TFL (A) and sub-TFL (B) isotopic compositions, (ii) mass-independent sub-TFL isotopic variations (C & D) and (iii) mass-dependent supra-TFL isotopic variations (E & F). The Terrestrial Fractionation Line (TFL, blue line) and Primitive Chondrule Minerals line (PCM, red line) are shown for reference. Errors are 2SD.

Fig 5: (A) Oxygen isotopic compositions of all olivine crystals measured in the 47 selected chondrules and IOGs in chondrites NWA 5206 and Piancaldoli. (B) Oxygen isotopic compositions of olivine grains in chondrules with average $\Delta^{17}O < 0‰$ (red circles) and those with $\Delta^{17}O > 0‰$ (black circles). The former show mass-independent isotopic variations whereas the latter display mass-dependent isotopic variations. The Terrestrial Fractionation Line (TFL, blue line) and Primitive Chondrule Minerals line (PCM, red line) are shown for reference. Errors are 2SD.

Fig 6: Oxygen isotopic compositions (expressed as $\Delta^{17}O$) reported as a function of (A) Mg# and incompatible element concentrations: (B) Al, (C) Cr, (D) Mn, (E) Ca, and (F) Ti. Chondrules with high Mg# and low concentrations of incompatible elements have variable, and commonly negative, $\Delta^{17}O$ values.

Fig 7: Average oxygen isotopic compositions of chondrules in chondrites NWA 5206 and Piancaldoli as functions of their (A) average Mg# and (B) surface areas.

Fig 8: Average $\Delta^{17}O$ values of chondrules as a function of their surface areas in chondrites NWA 5206, Piancaldoli, Semarkona, Bishunpur, Chainpur, Dar al Gani 369, Dar al Gani 378,

905 Dar al Gani 327, and Dar al Gani. Data from this study, Russell et al., 1996, 1998; Pack et al.,
906 2004; Kita et al., 2010; Ebert et al., 2018; Piralla et al., 2021; Siron et al. 2022.
907
908 **Fig 9:** Average $\Delta^{17}O$ values of chondrules as a function of their respective surface areas in
909 ordinary and Rumuruti chondrites. Data from this study, Pack et al., 2004; Kita et al., 2010;
910 Ebert et al., 2018; Piralla et al., 2021; Regnault et al., 2022.
911
912 **Fig 10:** Oxygen isotopic compositions (expressed as $\Delta^{17}O$) of *sub-TFL* (open black circles)
913 and *supra-TFL* (open red circles) chondrules reported as a function of (A) Mg# and
914 incompatible element concentrations: (B) Al, (C) Cr, (D) Mn, (E) Ca, and (F) Ti. Also
915 reported are host (open blue diamonds) and relict (open green diamonds) olivine grains from
916 larger OC chondrules (Piralla et al., 2021).

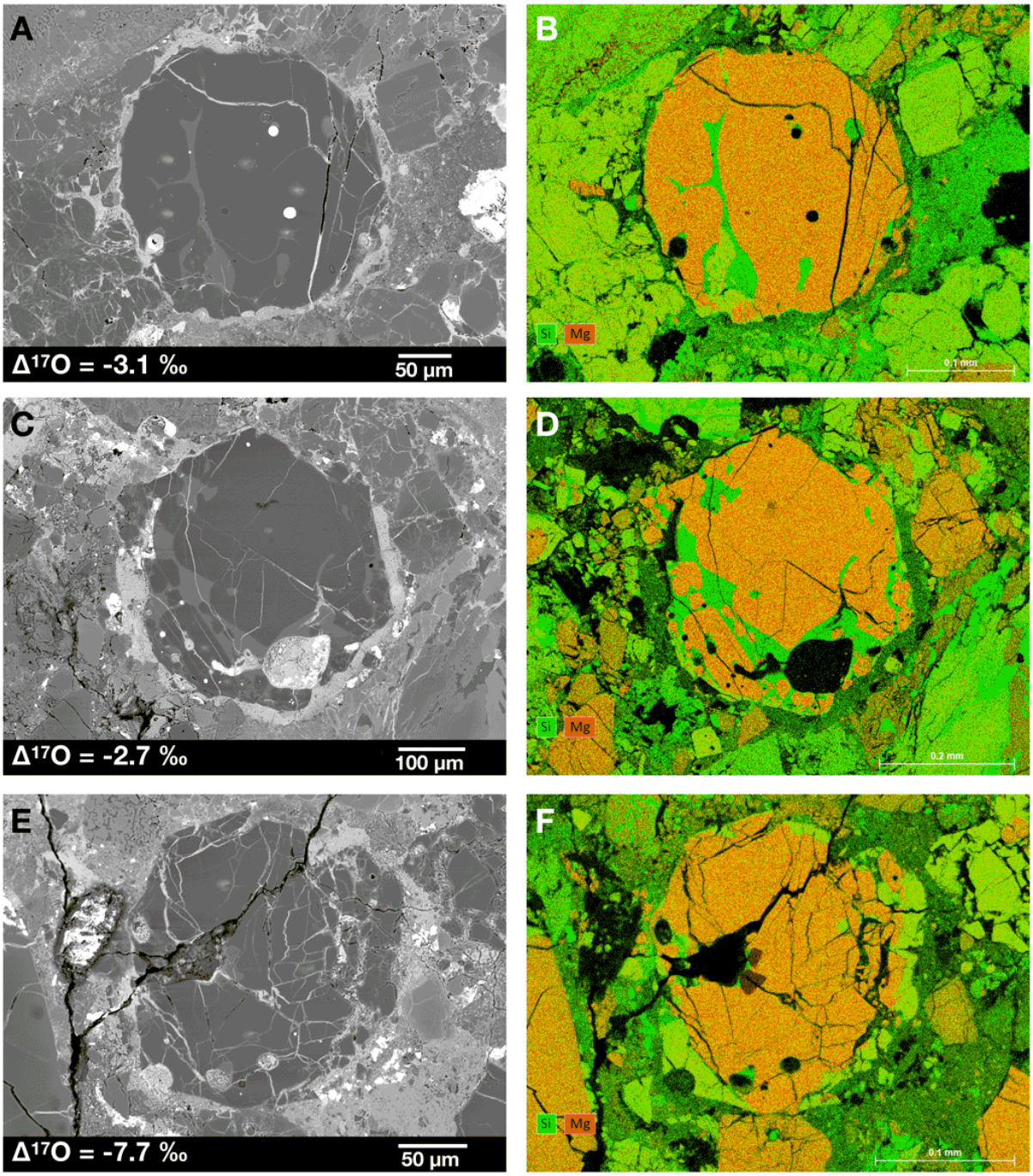
A
Δ17O = -3.1 ‰
50 µm
B
Si
Mg
0.1 mm
C
Δ17O = -2.7 ‰
100 µm
D
Si
Mg
0.2 mm
E
Δ17O = -7.7 ‰
50 µm
F
Si
Mg
0.1 mm

Fig. 1

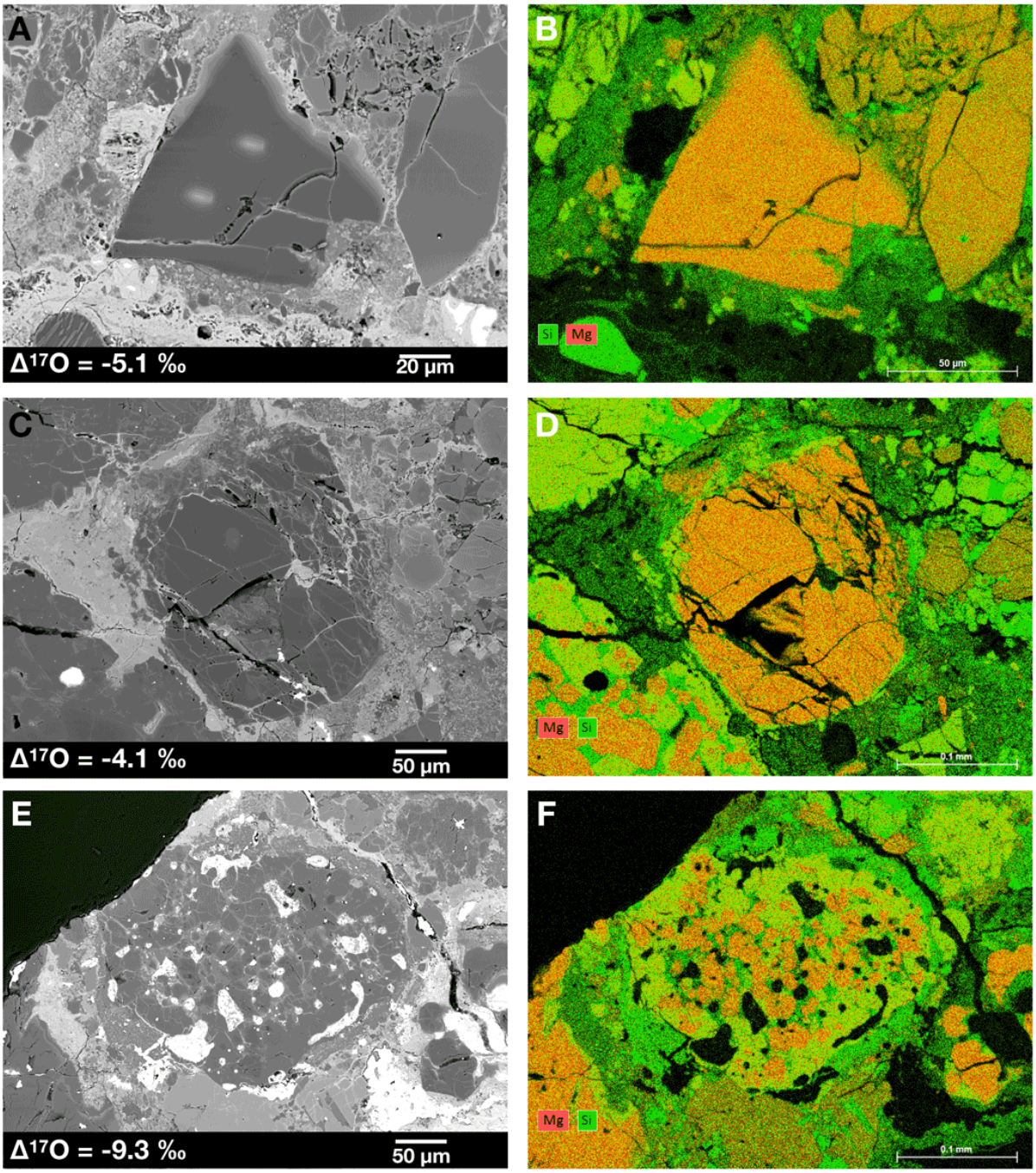
A
Δ17O = -5.1 ‰
20 µm
B
Si
Mg
50 µm
C
Δ17O = -4.1 ‰
50 µm
D
Mg
Si
0.1 mm
E
Δ17O = -9.3 ‰
50 µm
F
Mg
Si
0.1 mm

Fig. 2

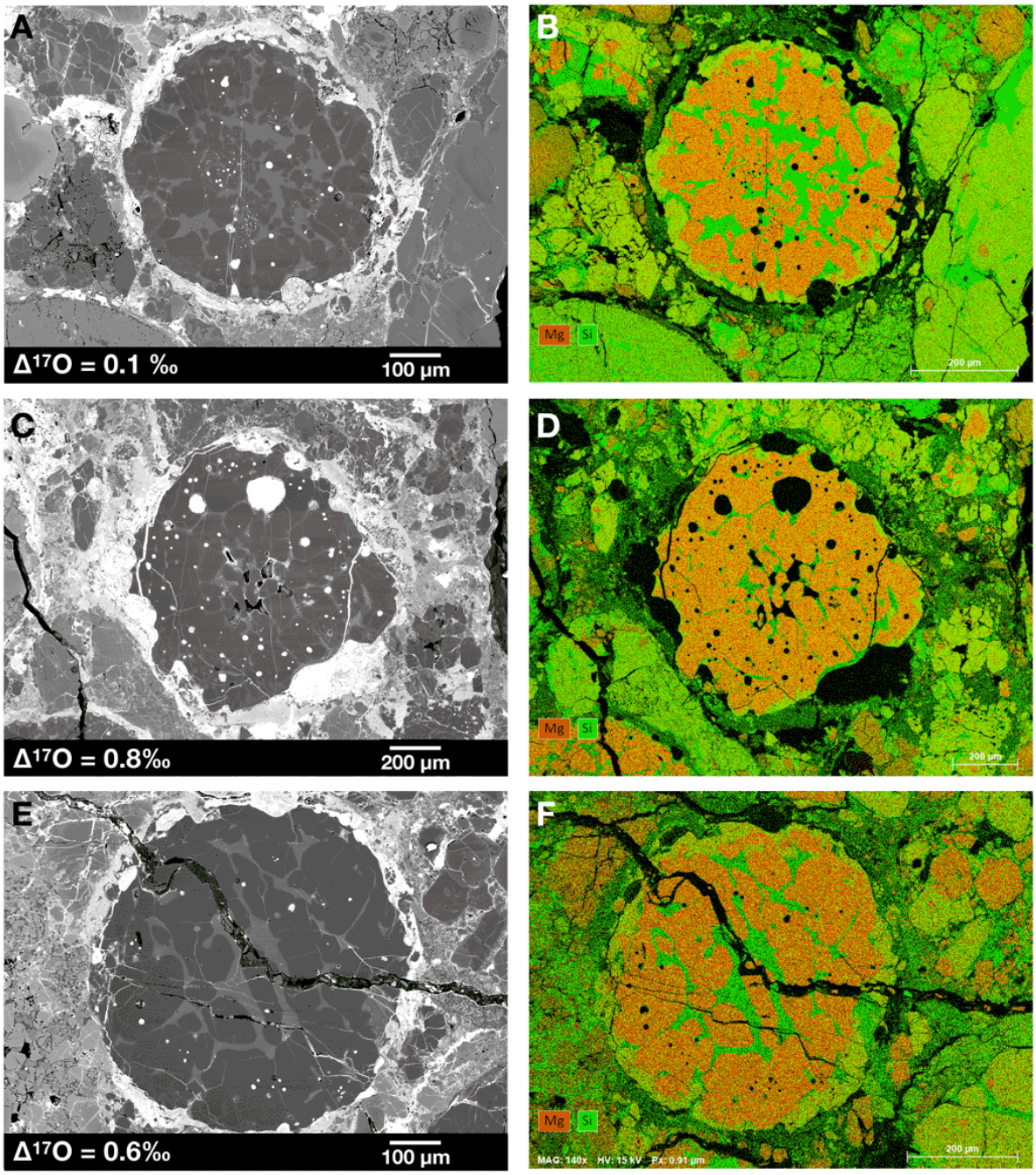
A
Δ17O = 0.1 ‰
100 µm
B
Mg
Si
200 µm
C
Δ17O = 0.8‰
200 µm
D
Mg
Si
200 µm
E
Δ17O = 0.6‰
100 µm
F
Mg
Si
MAG: 140x HV: 15 kV Px: 0.91 µm
200 µm

Fig. 3

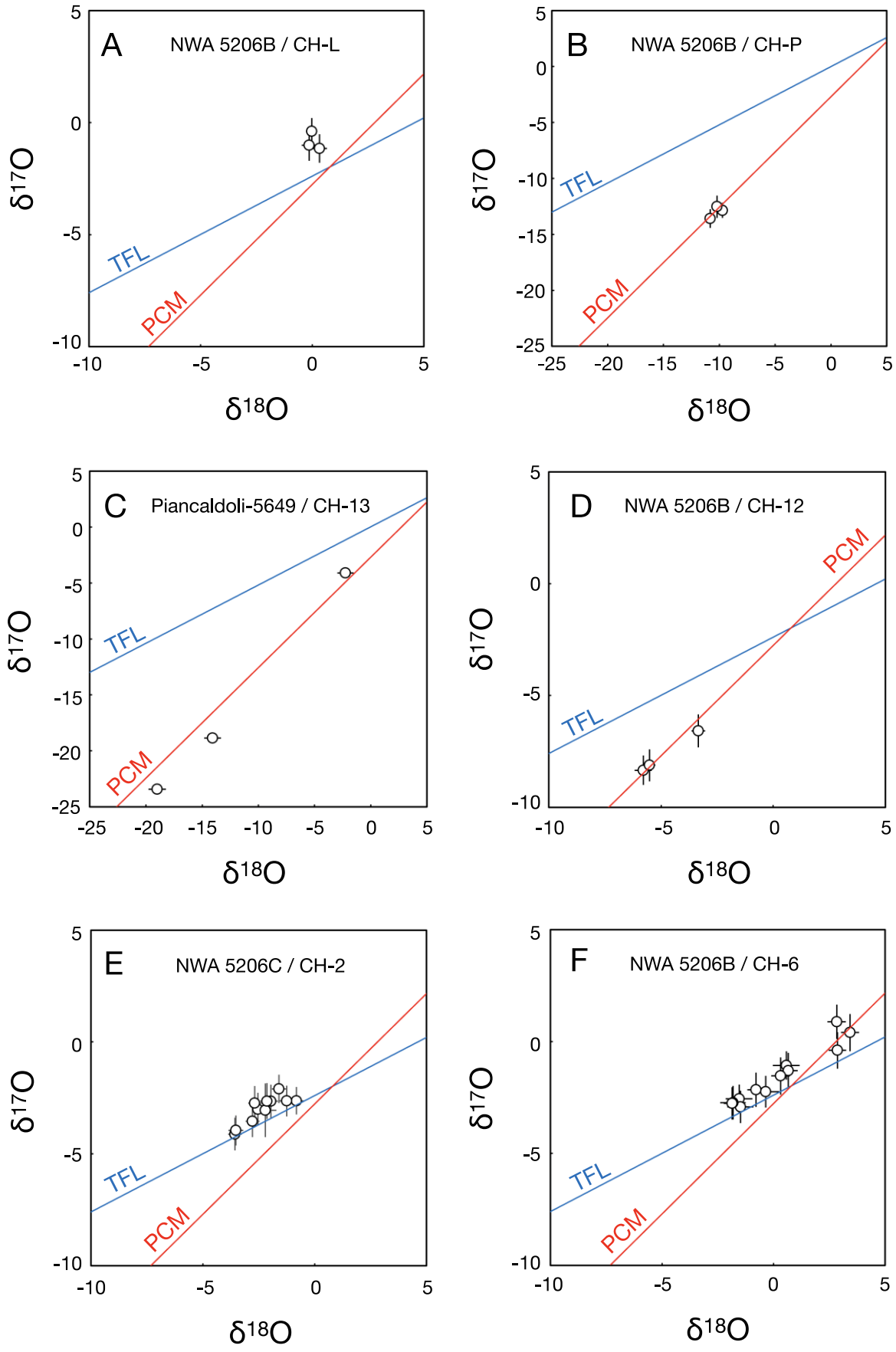
A
NWA 5206B / CH-L
B
NWA 5206B / CH-P
C
Piancaldoli-5649 / CH-13
D
NWA 5206B / CH-12
E
NWA 5206C / CH-2
F
NWA 5206B / CH-6
TFL
PCM
δ17O
δ18O

951
952

Fig. 4

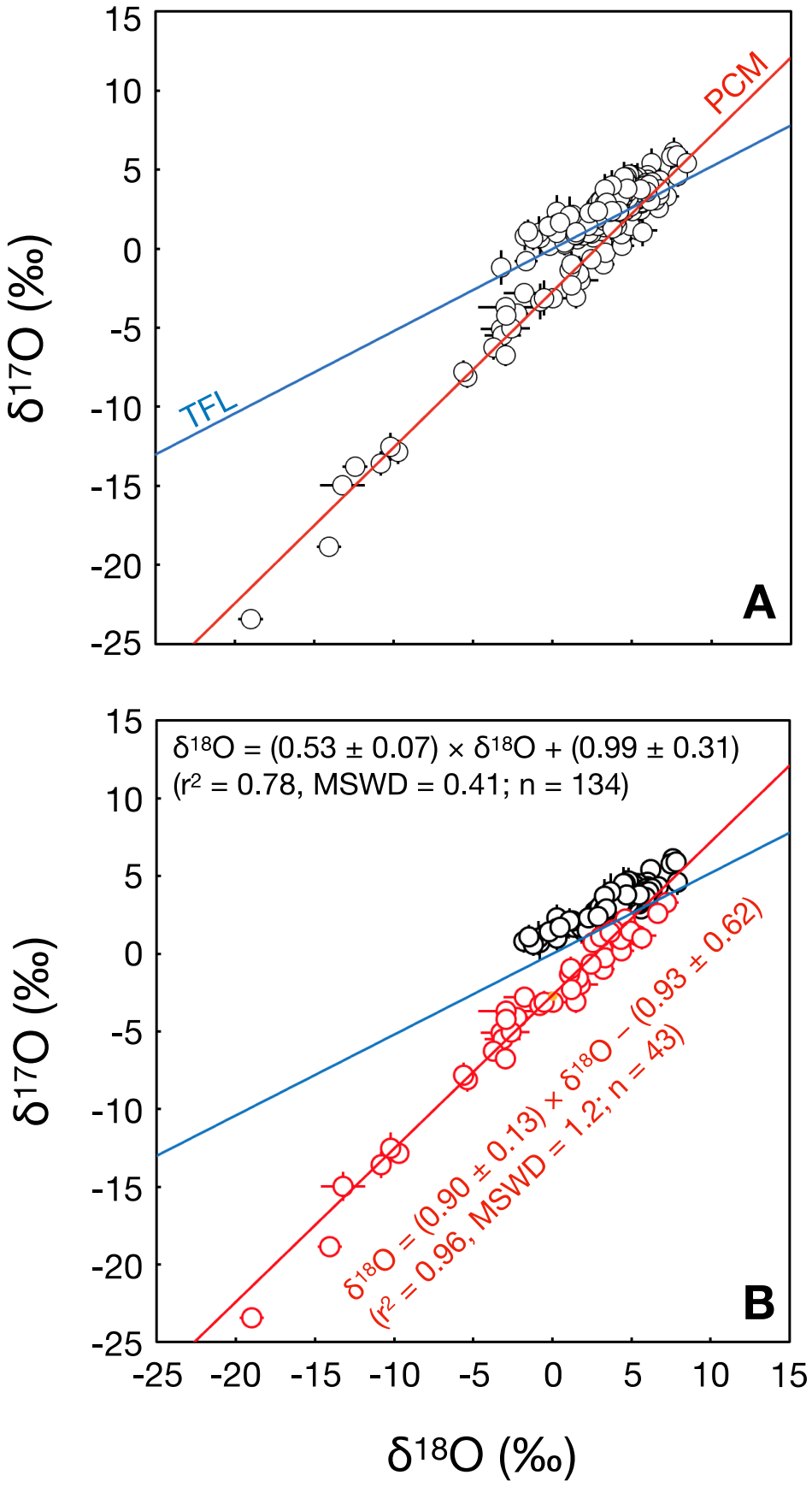

953
954
955

Fig. 5

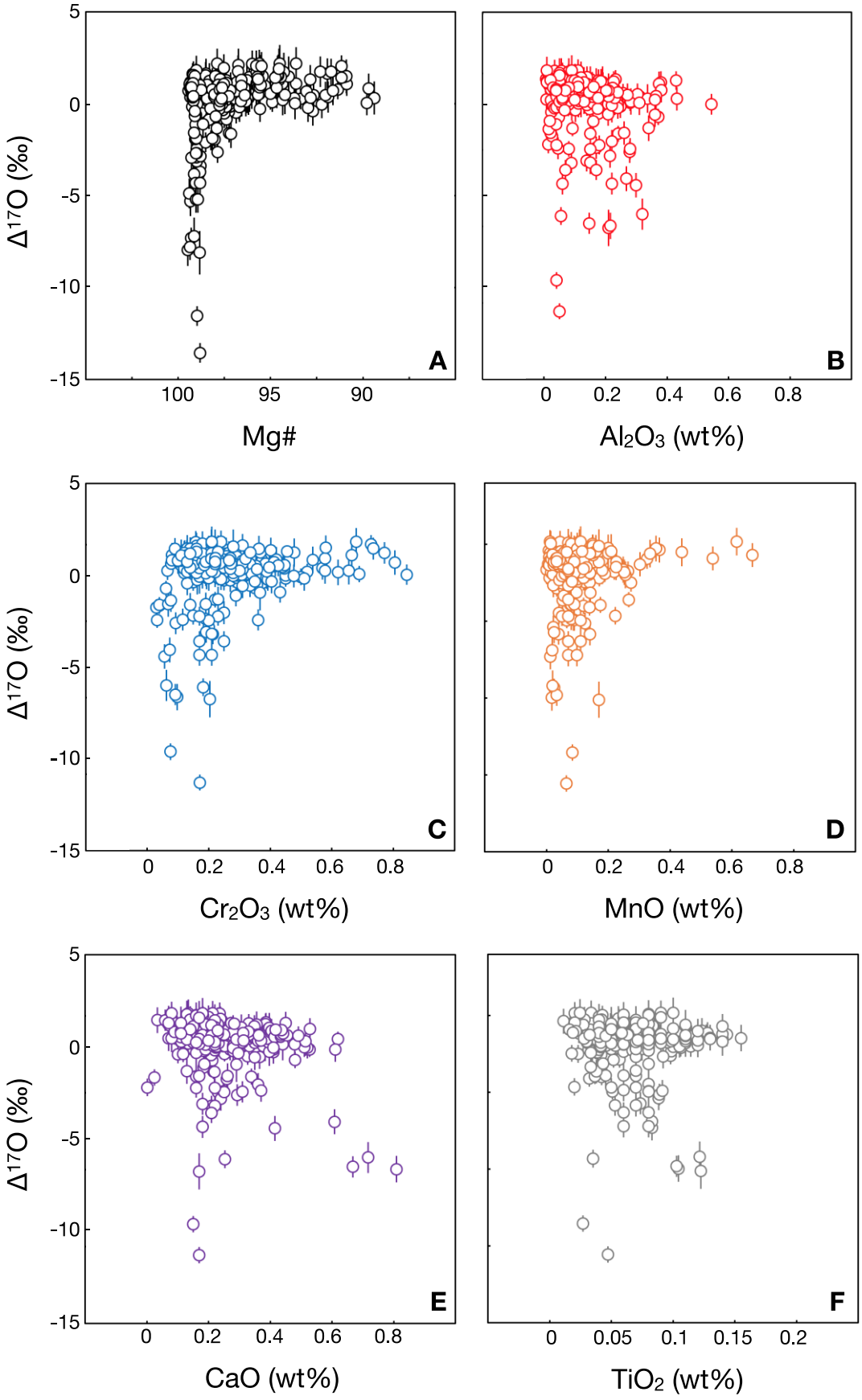
Δ17O (‰)
5
0
-5
-10
-15
A
100
95
90
Mg#
B
0
0.2
0.4
0.6
0.8
Al2O3 (wt%)
C
Cr2O3 (wt%)
D
MnO (wt%)
E
CaO (wt%)
F
0
0.05
0.1
0.15
0.2
TiO2 (wt%)

956
957

Fig. 6

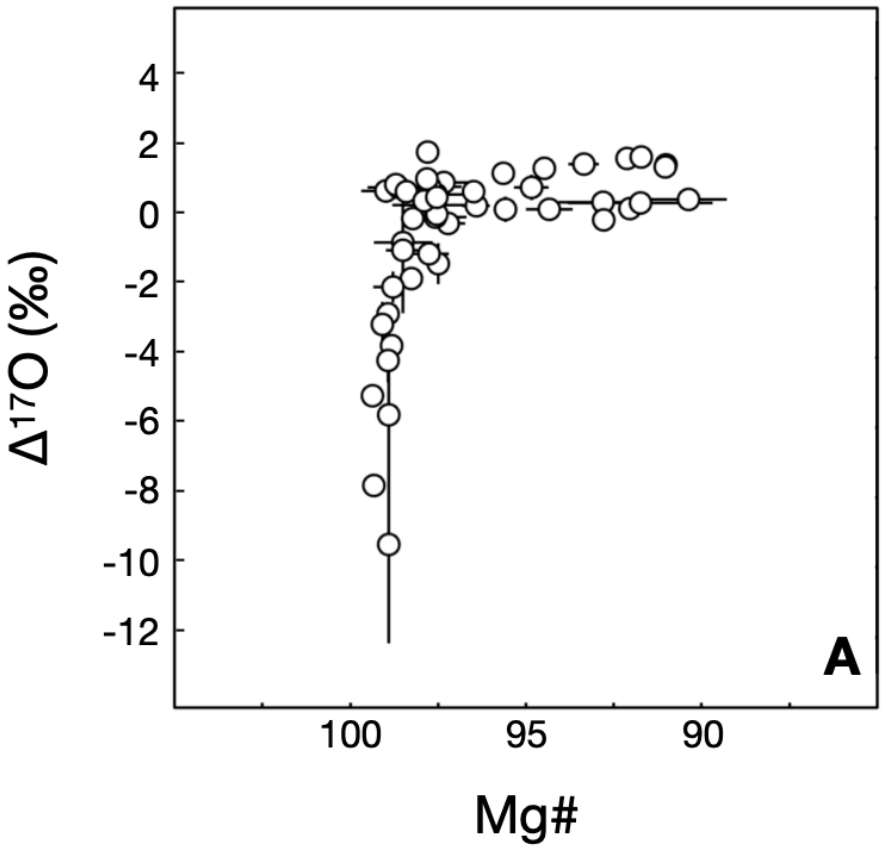
4
2
0
-2
-4
-6
-8
-10
-12
Δ17O (‰)
100
95
90
Mg#
A

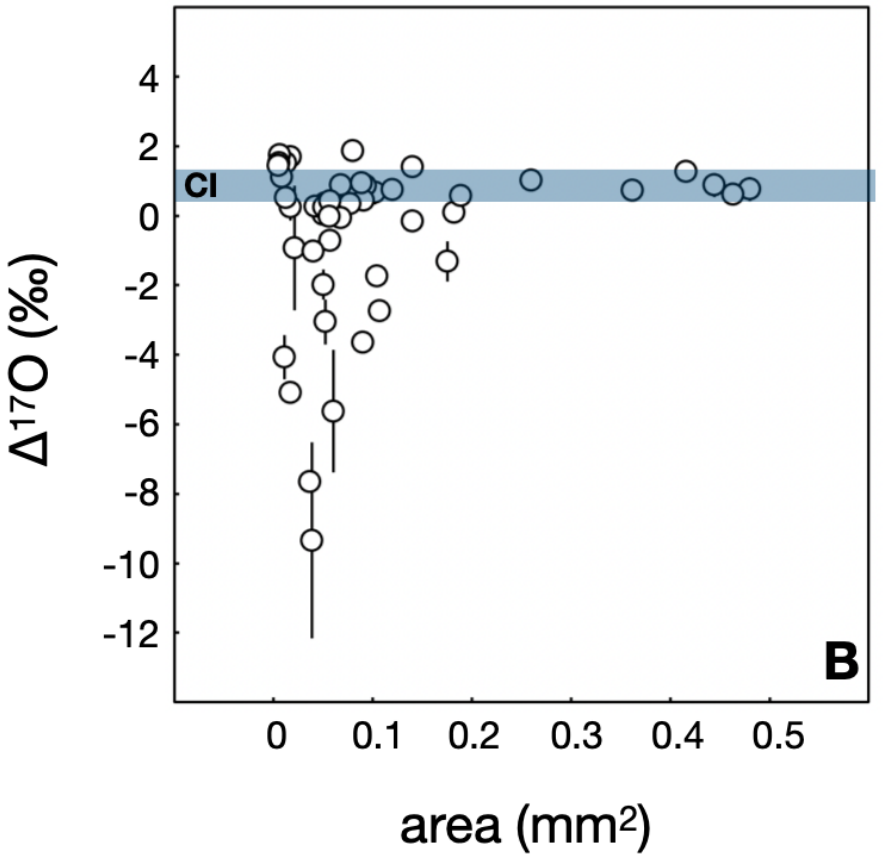
4
2
0
-2
-4
-6
-8
-10
-12
Δ17O (‰)
CI
0
0.1
0.2
0.3
0.4
0.5
area (mm2)
B

958
959

Fig. 7

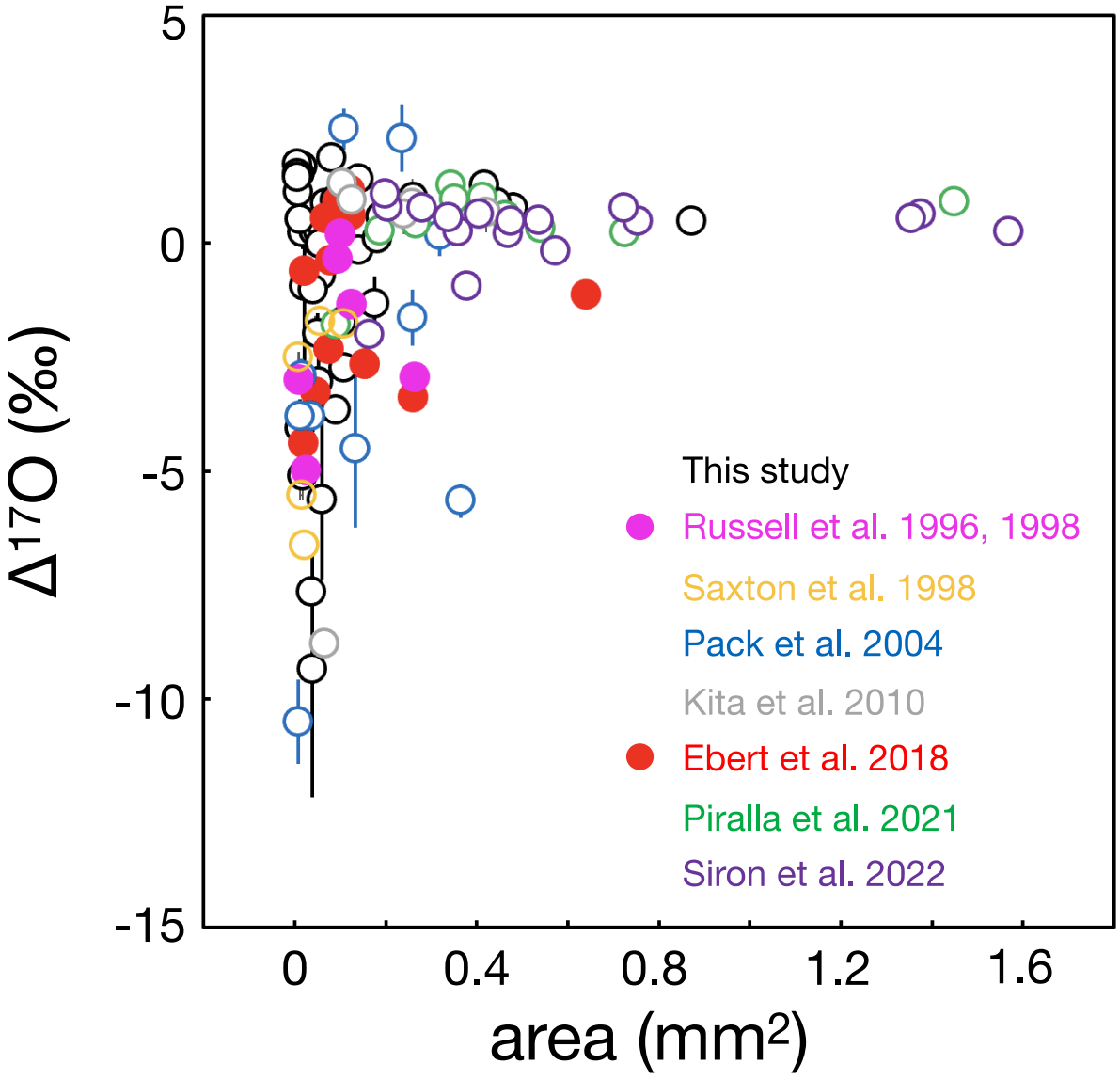
5
0
-5
-10
-15
Δ17O (‰)
0
0.4
0.8
1.2
1.6
area (mm2)
This study
Russell et al. 1996, 1998
Saxton et al. 1998
Pack et al. 2004
Kita et al. 2010
Ebert et al. 2018
Piralla et al. 2021
Siron et al. 2022

Fig. 8

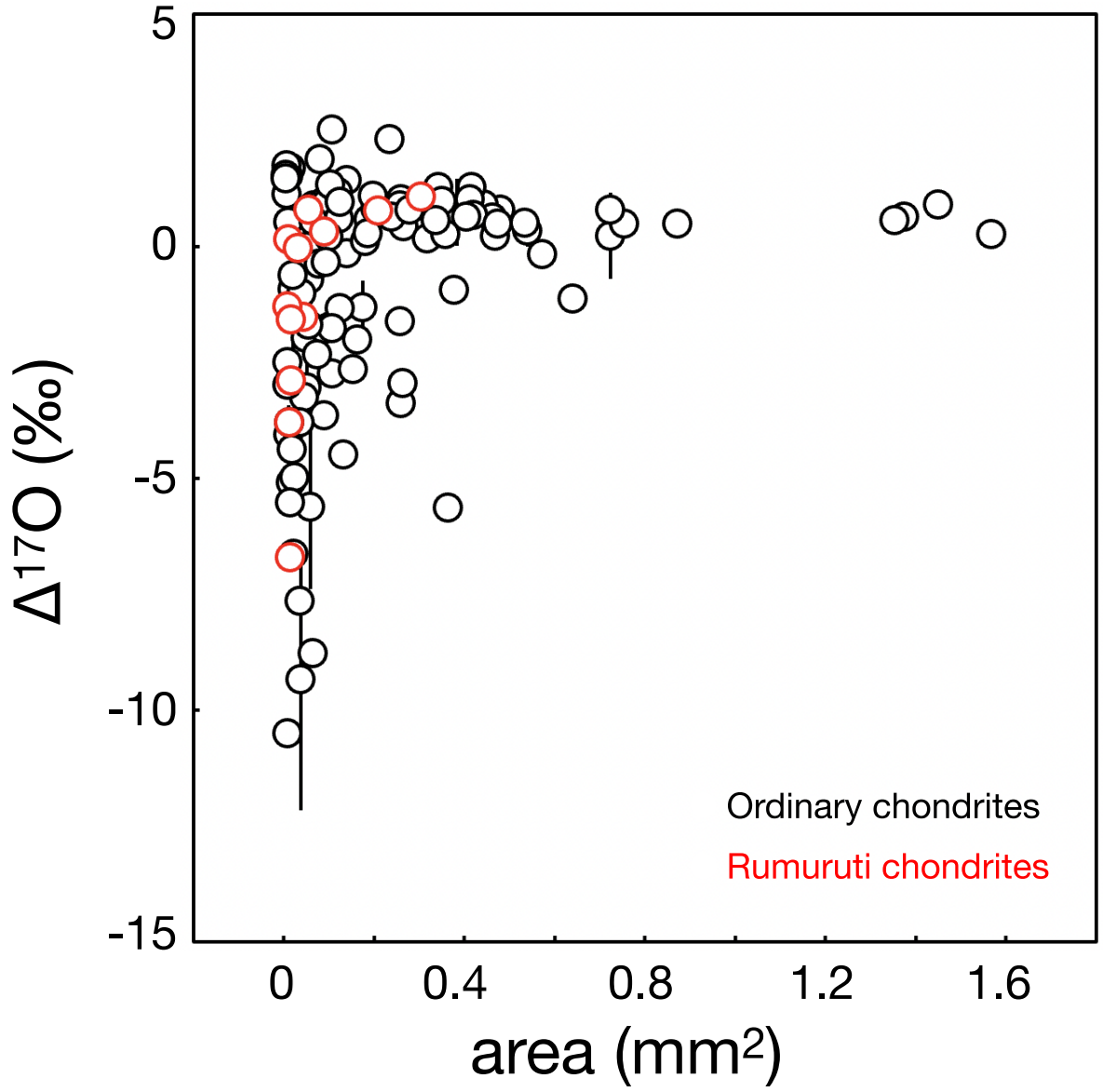
5
0
-5
-10
-15
Δ17O (‰)
0
0.4
0.8
1.2
1.6
area (mm2)
Ordinary chondrites
Rumuruti chondrites

Fig. 9

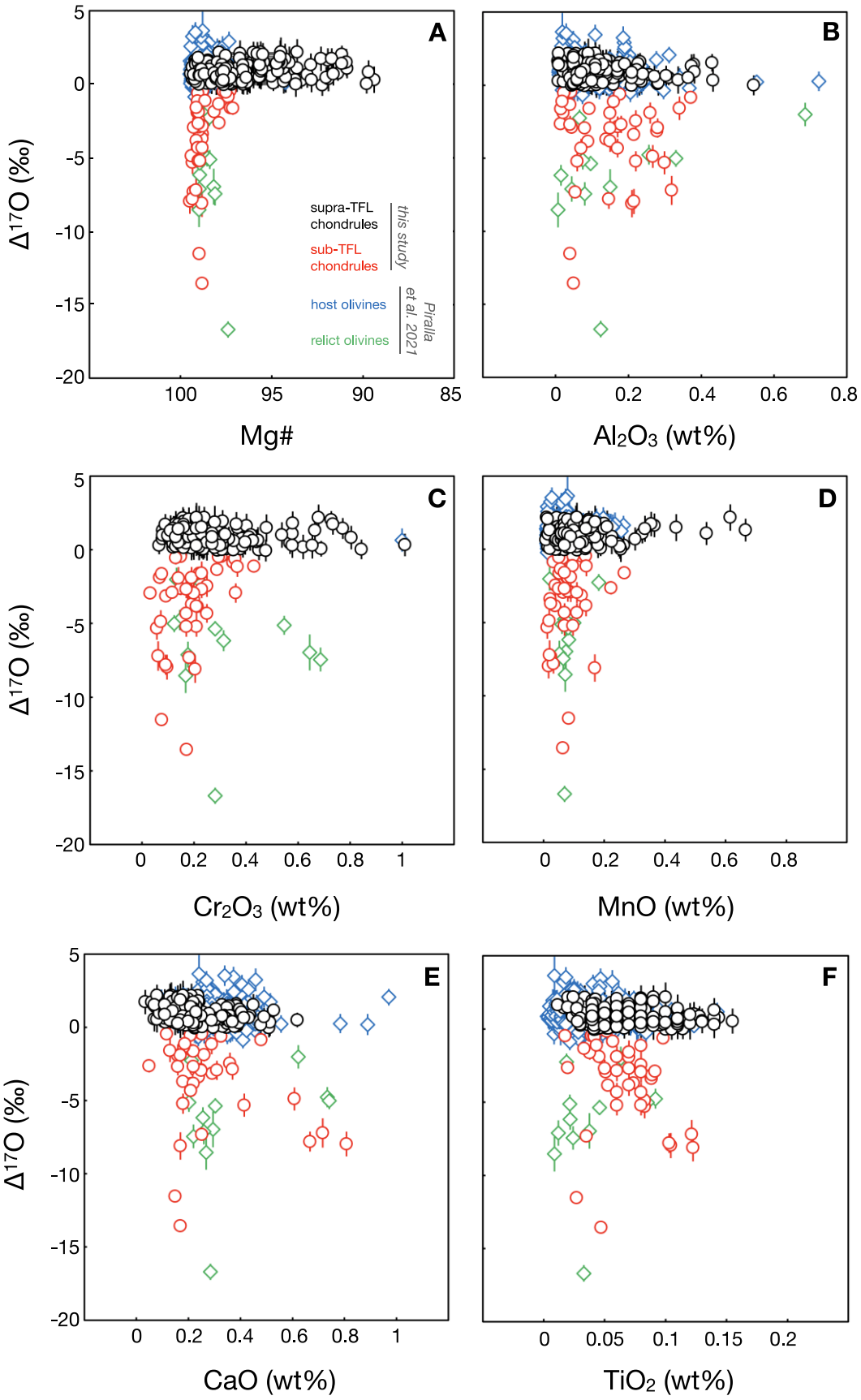
A
B
C
D
E
F
supra-TFL chondrules
sub-TFL chondrules
host olivines
relict olivines
this study
Piralla et al. 2021
Δ17O (‰)
Mg#
Al2O3 (wt%)
Cr2O3 (wt%)
MnO (wt%)
CaO (wt%)
TiO2 (wt%)

Fig. 10